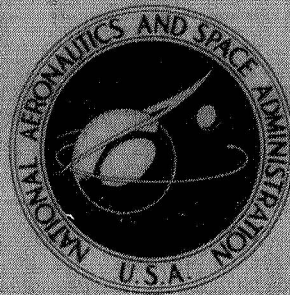


**NASA TECHNICAL
MEMORANDUM**



NASA TM X-2982

NASA TM X-2982

**SOME INJECTOR ELEMENT DETAIL EFFECTS
ON SCREECH IN HYDROGEN-OXYGEN ROCKETS**

*by Ned P. Hannum, Louis M. Russell, David W. Vincent,
and E. William Conrad*

*Lewis Research Center
Cleveland, Ohio 44135*

1. Report No. NASA TM X-2982	2. Government Accession No.	3. Recipient's Catalog No.	
4. Title and Subtitle SOME INJECTOR ELEMENT DETAIL EFFECTS ON SCREECH IN HYDROGEN-OXYGEN ROCKETS		5. Report Date February 1974	6. Performing Organization Code
		8. Performing Organization Report No. E-7512	
7. Author(s) Ned P. Hannum, Louis M. Russell, David W. Vincent, and E. William Conrad		10. Work Unit No. 502-24	11. Contract or Grant No.
9. Performing Organization Name and Address Lewis Research Center National Aeronautics and Space Administration Cleveland, Ohio 44135		13. Type of Report and Period Covered Technical Memorandum	
		14. Sponsoring Agency Code	
12. Sponsoring Agency Name and Address National Aeronautics and Space Administration Washington, D. C. 20546		15. Supplementary Notes	
16. Abstract <p>An experimental investigation was conducted at the Lewis Research Center to learn more about how the specific details of a concentric tube injection element affect the screech characteristics of a hydrogen-oxygen rocket engine. The four variables investigated were (1) impingement angle, (2) oxidizer tube blunt base thickness, (3) oxidizer tube recess and extension, and (4) oxidizer tube-annulus concentricity. Tests were made using a 27.34-cm (10.77-in.) diameter heat-sink combustor at nominally 2.06×10^6-N/m² (300-psia) chamber pressure. All of the test variables were investigated using a 157 element circular pattern injector. Additional oxidizer tube recess tests were made with a 421 element hexagonal pattern injector. Tests were conducted over the oxidant-fuel ratio range of 4 to 6. Stability evaluation for each configuration was made using the hydrogen temperature rating technique. Several element configurations were also cold flow tested using nitrogen and water as simulants. The element detail changes resulted in changes in hydrogen injector pressure drop even though the physical injection area was constant for all similar tests in both hot firing and cold flow tests. These changes in injector pressure drop produced changes in combustion stability. The data were correlated with a modified version of a previously reported injection area ratio correlation. By interpreting changes in injector pressure drop as changes in injector hydrogen flow resistance, the data were compared with a hydrogen flow response stability model and were found to be in agreement.</p>			
17. Key Words (Suggested by Author(s)) Screech Hydrogen-oxygen Injector element detail Instability		18. Distribution Statement Unclassified - unlimited Cat. 28	
19. Security Classif. (of this report) Unclassified	20. Security Classif. (of this page) Unclassified	21. No. of Pages 39	22. Price* \$3.00

SOME INJECTOR ELEMENT DETAIL EFFECTS ON SCREECH IN HYDROGEN-OXYGEN ROCKETS

by Ned P. Hannum, Louis M. Russell, David W. Vincent, and E. William Conrad
Lewis Research Center

SUMMARY

An experimental investigation was conducted at the Lewis Research Center to learn more about how the specific details of a concentric tube injection element affect the screech characteristics of a hydrogen-oxygen rocket engine. The four variables investigated were (1) impingement angle, (2) oxidizer tube blunt base thickness, (3) oxidizer tube recess and extension, and (4) oxidizer tube-annulus concentricity. Tests were made using a 27.34-centimeter- (10.77-in.) diameter heat-sink combustor at nominally 206×10^6 -N/m² (300-psia) chamber pressure. All of the test variables were investigated using a 157 element circular pattern injector. Additional oxidizer tube recess tests were made with a 421 element hexagonal pattern injector. Tests were conducted over the oxidant-fuel ratio range of 4 to 6. Stability evaluation for each configuration was made using the hydrogen temperature rating technique. Several element configurations were also cold flow tested using nitrogen and water as simulants.

The element detail changes resulted in changes in hydrogen injector pressure drop even though the physical injection area was constant for all similar tests in both hot firing and cold flow tests. These changes in injector pressure drop produced changes in combustion stability. The data were correlated with a modified version of a previously reported injection area ratio correlation. By interpreting changes in injector pressure drop as changes in injector hydrogen flow resistance, the data were compared with a hydrogen flow response stability model and were found to be in agreement.

INTRODUCTION

As evidenced by the extensive and costly development programs often required in achieving flight qualification, the rational design of injectors for new liquid bipropellant rocket engines remains a largely unfulfilled objective. This objective has nearly been

attained in certain instances; for example, with the large-scale concentric tube injector for the M-1 engine program (ref. 1), Preliminary Flight Rating Test performance and very stable combustion were attained with the first full-scale test configuration. For hydrogen-oxygen propellants and concentric-tube-type injector elements, substantial knowledge has been accumulated, and this information was fully exploited in arriving at the M-1 design configuration. Nevertheless, considerable judgment was required to bridge gaps in existing knowledge. In addition, certain detail design variables of potential importance had to be chosen with little or no information regarding their potential effects on stability and performance. This work was undertaken to resolve certain of these injector element design detail effects on stability.

Because of its high performance, ease of fabrication, and uniform combustion characteristics, the concentric-tube-type injector element was selected for an intensive and continuing study of screech at the Lewis Research Center using hydrogen-oxygen propellants. Reference 2 is an interim summary report on this effort. Also, injector elements of this type are presently used in flight engines such as the RL-10 and J-2, that use hydrogen-oxygen propellants. The major objective of the work reported herein is to provide design guidance relating the stability to variations in the injector element details believed to be significant. The experimental data are correlated with previously published stability data. The present data are also compared with a stability model proposed by Feiler and Heidmann in reference 3. Because of the significant role of injector flow coefficient C_d in determining the stability of a combustor, cold flow tests using nitrogen and water as propellant simulants were made and the data are compared with engine firing results.

The following element detail variables were investigated experimentally over the ranges indicated:

- (1) Injector impingement angle, deg 0 to 45
- (2) Oxidizer tube blunt base thickness, cm (in.) 0.0349 to 0.173
(0.01375 to 0.06800)
- (3) Oxidizer tube recess and extension, cm (in.) 1.27 (recess) to
3.18 (extension) (0.5 to 1.25)
- (4) Oxidizer tube eccentricity

The tests were conducted using a 0.274-meter (10.77-in.) diameter heat-sink combustor at a nominal chamber pressure of 2.06×10^6 N/m² (300 psia), resulting in a thrust level of about 89 000 newtons (20 000 lb). The high frequency combustion instability (screech) characteristics were determined using the hydrogen temperature ramping technique discussed in reference 4.

APPARATUS

Test Facility

The investigation was conducted at the Lewis Research Center Rocket Engine Test Facility. This is a 220 000-newton (50 000 lb) sea-level rocket test stand equipped with an exhaust gas muffler and scrubber. The rocket engines were mounted on a thrust stand to fire vertically into the scrubber. The facility used pressurized propellant storage tanks to supply the propellants to the rocket engine.

The engine test stand is shown in figure 1. A mixing tube to vary the temperature of the hydrogen to the engine was located in the section of line just downstream of the liquid hydrogen and gaseous hydrogen engine fire valves.

Engine

The rocket engine (fig. 2) was comprised of an injector, a cylindrical 0.274-meter (10.77-in.) inside diameter heat-sink-type thrust chamber 0.432 meter (17 in.) long, and a convergent-divergent heat-sink exhaust nozzle. The nozzle had a throat area of 0.0309 square meter (47.91 sq in.) and a contraction ratio of 1.89. The expansion ratio was 1.3. The inner surfaces of the combustion chamber and exhaust nozzle were coated with 0.772 millimeter (0.030 in.) of flame-sprayed zirconium oxide to reduce the heat transfer to the metal. The thrust chambers could be operated for 3 seconds without damage. This run duration was adequate to obtain the desired test results.

Injectors

The injectors used in this investigation were of the concentric-tube-type with each element consisting of a central oxidizer tube surrounded by a concentric hydrogen annulus. A basic 157 element circular pattern injector was used to evaluate effects of the (1) impingement angle, (2) oxidizer tube blunt base thickness, (3) oxidizer tube recess and extensions, and (4) element concentricity. Configuration changes were accomplished by installing sets of removable injector elements into standard injector bodies. Additional oxidizer tube recess tests were made using a 421 element hexagonal pattern injector. Faceplate view photographs of the two injectors are shown in figure 3 and dimensioned sketches of the various injector elements are shown in figure 4. These injector details will be discussed in a later section.

Hydrogen Temperature Control

The hydrogen temperature ramp used to determine the screech limits was accomplished by varying the proportions of 263 K (50° R) liquid hydrogen and ambient temperature gaseous hydrogen in the mixing tube while maintaining a constant total flow rate. Mixing was accomplished by swirling the liquid into the gaseous hydrogen stream. The mixing section was 4 feet long and was located just upstream of the injector. The constant oxidant-fuel ratio was maintained by an automatic controller.

Test Control

Three set point inputs were required for the automatic controller - chamber pressure, oxidant-fuel ratio, and temperature ramp rate. The oxidizer flow rate was controlled by a closed loop system which sensed the chamber pressure. The liquid hydrogen and gaseous hydrogen flow rates were summed and the total was controlled by adjusting the liquid hydrogen flow rate to satisfy the oxidant-fuel ratio. The gaseous hydrogen flow rate was controlled by a closed loop system which sensed the temperature ramp rate selection.

Cold Flow Apparatus

The cold flow apparatus consisted of a one-element injector section which discharged into a pressure chamber. The element was mounted to flow the water and nitrogen simulants vertically downward. Plastic windows in the chamber permitted observation of the simulated propellant injection behavior. Valves and pressure regulators in the supply lines were used for varying flows. The tank was equipped with back pressure regulators to maintain the preset simulated chamber pressure.

Hot Firing Instrumentation

Location of the various transducers and the associated engine plumbing are shown by the schematic diagram of figure 5. Except for the high-frequency pressure response types, the transducer signals were transmitted to an automatic digital data recording system. To allow identification of the screech mode and to determine the character and phase relations of the pressure field, piezoelectric-type, water-cooled, flush mounted pressure transducers were used. The amplitude response characteristics of the trans-

ducers as installed are flat to within 10 percent up to a frequency of 6000 hertz and have a nominal resonant frequency of 130 000 hertz. The high-frequency signals were recorded on magnetic tape in analog form and were also displayed on direct reading instruments in the control room for visual monitoring during the tests.

The liquid oxygen flow rate was determined with a calibrated turbine-type flowmeter. The liquid hydrogen flow rate was measured using a venturi submerged in the supply tank and the gaseous hydrogen flow rate was measured using an orifice plate. The liquid propellant temperatures were measured with the platinum resistance-type sensors described in reference 5. The hydrogen injection temperature was measured using four carbon resistance-type probes (ref. 6) installed as shown in figure 2. The pressure and temperature systems were calibrated immediately prior to data acquisition by an electrical two-step calibration system which used resistances in an electrical circuit to simulate given conditions.

Cold Flow Instrumentation

The cold flow rig instrumentation consisted of strain gage pressure transducers, two turbine water flowmeters, and a venturi for measuring nitrogen flow. Data were recorded on a photographic-paper-type oscillograph. A two-step calibration was made before and after each test.

PROCEDURE

In reference 4, it was established that decreasing the hydrogen injection temperature could lead to unstable combustion in hydrogen-oxygen engines and that the hydrogen temperature at which instability occurred was a good indicator of the sensitivity of the engine to screech. The hydrogen temperature at which combustion instability occurred, called the transition temperature, is therefore a convenient parameter for determining the relative stability of various engine configurations and was used in the present investigation. Lower transition temperatures indicate increased stability. A temperature ramping technique was employed to determine the transition temperature.

Temperature ramping rates up to 26 K per second (50° R/sec) were possible with only small variations in the oxidant-fuel ratio. If by the initial ramping technique the configuration was stable to the minimum hydrogen temperature available with the facility, subsequent runs were made using only the liquid hydrogen at approximately 28 K (54° R).

The combustion performance was determined for a range of hydrogen injection temperatures by making several runs at essentially constant temperature and analyzing the

data obtained at the end of the steady-state period just prior to shutdown.

Engine ignition was accomplished after hydrogen flow was established by injecting a small amount of fluorine into the oxidizer line immediately upstream of the injector simultaneously with actuation of the oxidizer engine valve. Tests were conducted over an oxidant-fuel range of 4 to 6.

The temperature ramping technique made it difficult to determine an accurate value of the instantaneous mass flow of hydrogen from the injector. Because of the large change in hydrogen density with temperature, a significant mass of hydrogen was accumulated in the mixing tube during the temperature ramp. As a result, the instantaneous oxidant-fuel ratios of the injector varied from the mean set value for those runs using the temperature ramp technique.

Although the facility was equipped with a thrust measuring system, the measurements obtained were not considered sufficiently accurate to present. The characteristic exhaust velocity C^* based on the chamber pressure was used instead to compare the performance of the various injectors. The chamber pressure was corrected for the momentum pressure loss by the method of Huff, Fortini, and Gordon in reference 7. The characteristic exhaust velocity efficiency ηC^* was based on the theoretical value for equilibrium expansion obtained from the calculations of Gordon and McBride in reference 8. Engine performance data are considered to be accurate to within ± 2 percent.

Cold flow tests were performed on single elements using ambient temperature nitrogen gas to simulate hydrogen, and water to simulate liquid oxygen. During the cold flow tests, both the nitrogen and water were flowed simultaneously. These tests were made to isolate the strictly hydraulic effects and then observe whether or not the same trends occur as in the hot firing tests.

The cold flow tests were conducted by setting a desired nitrogen tank pressure and water flow. The injector nitrogen valve was then opened in steps to obtain steady flow and pressure data. The tank pressure remained constant throughout the nitrogen flow excursion.

RESULTS AND DISCUSSION

The following discussion presents the experimental injector pressure drop results from water flow tests along with actual hot firing test results for each of the variables investigated. Some of the hot firing results are correlated with an existing theoretical response factor model and are presented in a later section to provide a possible explanation for the effects obtained. All of the hot firing data are tabulated in table I and summarized in table II. The cold flow data are shown in table III. Inputs to the response factor model are shown in table IV.

Effect of Impingement Angle

In the study reported in reference 9, screech results from three different organizations were examined and compared with the Crocco stability theory. In all three cases, concentric tube elements were used with hydrogen-oxygen propellants. Only limited success was achieved in relating these results, quite possibly because of the variation of impingement angles (0° to 20°) in the data set. Thus, it appeared that impingement angle had an effect on screech characteristics, but due to other variables, cross comparisons could not be used to isolate the effect. In view of the need to resolve this question, a short series of tests were conducted using injectors with impingement angles of 0° , 15° , 30° , and 45° . All other variables (such as injection area ratio, element size, base thickness, and element spacing) were held constant. A detailed sketch of the elements used in the angle tests is shown in figure 4(a). The elements used for 0° impingement angle are the same as shown in figure 4(b) (standard base thickness).

The effects on the screech limit are shown in figure 6 where each of the data points represent transition into screech as the hydrogen injection temperature was ramped downward from higher (stable) levels. These data, tabulated in table II, were obtained at an oxidant-fuel ratio of 5.0 from cross plots of the data in table I.

As shown in figure 6(a), the stability limit is lowered 16 K (30° R) (stability increased) over the range of 0° to 45° impingement angle, thus illustrating the stabilizing effect of increased impingement.

By the method of testing, as the hydrogen temperature is lowered toward the screech limit, the density, of course, is being increased. At constant flow rate, hydrogen injection pressure drop decreases as density increases (refer to table I). This indicates that there may be a relation between injection ΔP and stability, implying the higher the injection ΔP , the more stable an injector will be. This will be discussed further in a later section on response factors.

The relation between impingement angle and injector flow coefficient is also presented along with the apparent effect on stability. The hot-firing information is shown in figure 6(b) where it is seen that hydrogen injector flow coefficient C_d decreases with increasing impingement angle. This reduction in effective flow area also means higher pressure drop across injector elements and thus higher hydrogen injector manifold pressure. For weight and pumping considerations, it is desirable to maintain supply pressure to the injector manifold as low as possible. Therefore, a designer may well be forced to compromise between the beneficial effects that increased impingement angle have on stability and the weight penalty which may be imposed because of the accompanying increased injector pressure drop. The use of high impingement angles may also present a fabrication difficulty. The difficulty arises from the fact that large injection angles allow very little margin of error in positioning each injector element. A very

slight difference in axial position of an oxidizer tube produces a relatively large change in hydrogen injection area which, of course, affects injector pressure drop. It would, therefore, be necessary to exercise extreme care in assuring proper axial position of each element.

As may be seen from figure 6(b), there is only a slight decrease in oxygen flow coefficient with increasing injection angle over the range investigated. This is not surprising since there was no physical change made to the oxygen flow passage. The only effect of injection angle on oxygen C_d would be the slight differences in the effect of the hydrogen stream impinging upon the oxygen stream.

The results of the cold flow simulation tests for impingement angle effects are shown in figure 6(d). The trend shown here is the same as that indicated in the hot firing case, with nitrogen C_d decreasing with increasing impingement angle as did hydrogen C_d . C_d 's were all based on a nitrogen flow rate of 27.25 grams per second (0.06 lb/sec). The rate of 27.25 grams per second (0.06 lb/sec) is nominally the mass flow rate per element of hydrogen through the 157 element injectors used in hot firings.

There was very little change in water C_d over the range of injection angles investigated as seen in table III. This trend agrees well with hot firing liquid oxygen C_d 's.

Flow coefficients for both hot firing tests and cold flow simulation tests were calculated using the following flow equation:

$$C_d = \frac{\dot{w}}{A(\rho \Delta P)^{1/2}}$$

where

\dot{w} fluid weight flow, kg/sec

A flow area, m^2

ρ fluid density, kg/m^3

ΔP injector pressure drop, N/m^2

For each run, \dot{w} and ΔP were measured, and the ρ used was the density corresponding to the temperature of the particular fluid involved. In hot firings, the conditions were taken at the instant before transition to screech.

The C_d for each individual run is shown in table I and the average C_d for each configuration is given in table II. Only C_d 's calculated from the data taken just before transition points are included in the averages. Averaging C_d 's calculated from several different runs is justified because C_d should be the same for any particular element configuration regardless of flow rate (O/F) as long as the Reynolds number is constant. In this program, hydrogen injection Reynolds number was always above 2 000 000 and

oxygen injection Reynolds number was always above 350 000. At these high values of Reynolds number, reference 10 indicates that C_d does not vary with Reynolds number.

Characteristic exhaust velocity efficiency based on chamber pressure is shown in figure 6(d) for each of the four injection angles tested. Within the accuracy of the measurement system, there appears to be no effect of injection angle on performance. Thus, it is seen that increased injection angle may be used to improve stability provided that the increased injector pressure drop is tolerable.

Effect of Oxidizer Tube Blunt Base Thickness

Careful reconsideration of a large matrix of configurations reported in reference 1 and also J-2 experience led to a suspicion that the blunt base width of the oxidizer tubes (uncontrolled prior to this time) might also play a significant role in stability. Since the previous configurations did not allow isolation of this variable, a series of three configurations was built and evaluated with the oxidizer tube base width varied from 0.0349 centimeter (0.01375 in.) (minimum wall thickness for pressure load) to 0.173 centimeter (0.06800 in.) (fig. 4(b)). All other factors known to influence stability, such as hydrogen injection area, were held constant.

Hydrogen transition temperature is shown in figure 7(a) as a function of oxidizer tube base width for operation at a mixture ratio of 5.0 (cross plotted). It is seen that the screech limit was changed slightly by the base width. The least stable configuration occurred at the intermediate width.

Figure 4(b) shows that the configuration changes were made by altering the final hydrogen orifice dimension to provide a constant injection area with each different oxidizer tube base thickness tested. The entrance orifice (hydrogen) was the same for all configurations. The final orifice has the same area for all configurations but different shapes, thus the flow passages were somewhat different in each case. The question remains as to whether the stability changes mentioned previously were due entirely to the changes in oxidizer-tube blunt base area or to changes in the flow characteristics of the hydrogen injector. The significance of the latter possibility will be emphasized in an instability theory to be discussed later.

The effect of base thickness on injector C_d is illustrated in figure 7(b) for the hot firings. Of the three thicknesses tested, the intermediate or standard thickness gave the highest C_d 's for both hydrogen and oxygen. Of course, the intermediate thickness was also the least stable as previously mentioned. This is consistent with the results found with impingement angle variation which indicated that low C_d (higher pressure drop) produces greater stability.

The results of cold flow simulation tests are tabulated in table III. Both nitrogen

and water C_d 's were constant for all base thicknesses tested. The contrast with hot firing results indicates that the effects of base thickness on C_d are not the simple hydraulic effects as observed with impingement angle data and, therefore, may not correlate with the other element detail data.

Combustion efficiency at a mixture ratio of 5.0 is shown in figure 7(c) for each configuration and indicates that oxidizer tube base thickness has little effect on performance over the range tested. The blunt area of such oxidizer tubes, however, is not well cooled and, although no metal erosion was found with these injectors, erosion damage would seem probable with increasing blunt base thickness, particularly at higher chamber pressures. From these data then, the preferred approach would be to make the blunt base as thin as is structurally possible.

Effects of Oxidizer Tube Recess and/or Extension

During the development program on the J-2 engine, it was found that recessing the oxidizer tubes below the surface of the faceplate improved engine combustion stability. To confirm this finding with much finer elements, a single value of recess 0.254 centimeter (0.10 in.) was evaluated at Lewis Research Center and again found to be effective in improving the screech limit (ref. 4). These previous data, however, provided no information regarding the optimum amount of recess for screech suppression. Accordingly, tests were run with injectors having nominal thrust per element of 22.7 and 59 kilograms (50 and 130 lb) for several values of tube recess. Figure 4(c) shows the dimensional detail of the 421 element injector elements used in the tests. The test results are given in figure 8. As the tubes were recessed from the flush condition, the hydrogen transition temperature decreased sharply (improved stability) with initial recess of approximately six tube diameters; after that, the temperature decreased more gradually (fig. 8(a)). At the maximum recess, 1.27 centimeters (0.5 in.), the configuration was stable with the minimum hydrogen injection temperature possible in the facility (29 K or 54° R).

The effect of oxidizer tube recess on C_d for hot firings of the fine element injector is shown in figure 8(b). A reduction in hydrogen C_d with oxygen tube recess is readily seen. Again, more stable operation coincides with low hydrogen C_d . There is only a slight reduction in oxygen C_d with increasing recess.

Oxygen tube extension effects were not investigated with this fine element injector. Cold flow tests also were not performed on the fine element injector, neither for recess nor extension.

Performance (fig. 8(c)) is seen to increase slightly with the initial recess to 0.254 centimeter (0.10 in.) and thereafter decrease as recess was increased further.

Thus, it is seen that for this injector family, most of the benefit was obtained with 0.238 centimeter (0.094 in.) recess. This amount of recess corresponds to approximately two tube internal diameters. However, recess depths to 1.27 centimeters (0.5 in.) could be used if stability was paramount and performance losses were tolerable.

As noted earlier, the larger injector elements (157 elements at 0° impinging angle) were run both with recess and with the oxidizer tubes extended beyond the face of the injector into the combustion chamber. The rationale for extension was that, if simply increasing the temperature of the hydrogen prior to combustion was stabilizing, maybe this could be accomplished by allowing the fuel to be heated in the combustion chamber before encountering the oxidizer. The delayed mixing could be caused by extending the oxidizer tubes into the combustion chamber. Details of these elements are shown in figure 4(d). The data on the tube extension were obtained to extend the data of reference 11 for a single value of 3.18 centimeters (1.25 in.), where it was found that stability was improved but at the expense of reduced performance.

Results for both recess and extension are shown on the same plot in figure 9(a). The conventional (flush) configuration encountered screech as the hydrogen temperature was reduced below 58.3 K (111° R). When the oxidizer tubes were recessed, the transition temperature decreased (stability improved) until at a recess of 0.888 centimeters (0.35 in.), a stable operation at minimum temperature was found. The amount of recess corresponding to stable operation is approximately six tube diameters. These stability results are similar to those for the finer elements of figure 8, but the shape of the curve was opposite in that the most rapid improvement was near the point of maximum recess in the coarse element case. From these data and the J-2 results, it may be concluded that recess may be used to improve combustion stability significantly for concentric tube elements between 22.7 and 83.7 kilograms (50 and 380 lb) of thrust per element, but the optimum recess for required stability and performance may depend upon element size.

Continuing beyond the flush configuration, tube extension up to 1.904 centimeters (0.75 in.) decreased stability (fig. 9(a)). However, a marked change in the character of the combustion apparently occurred when the tubes were extended further to 3.18 centimeters (1.25 in.). From a screech standpoint, the longest configuration was stable at minimum hydrogen temperature (about 29 K or 55° R). There was, however, some low frequency instability (chugging, 200 to 300 Hz) and the combustion was generally rough. Also, there was a reduction in combustion efficiency which will be discussed later.

The effects of oxidizer tube recess and extension on C_d for hot firings of the coarse element injector are shown in figure 9(b). A drastic reduction in flow coefficients with increasing recess can be readily seen, particularly in the hydrogen case. Hydrogen C_d 's as low as 0.3 resulted. The same figure shows that there was no variation in either hydrogen or oxygen C_d with increasing oxygen tube extension over the range investigated.

For cold flow tests of this injector configuration, nitrogen (fuel) C_d is shown in figure 9(c) to increase with increasing oxidizer tube recess. This is contrary to the trend observed with hot firing tests. Only one oxygen tube extension was tested in cold flow tests, that of 0.635 centimeter (0.25 in.). Figure 9(c) shows that this resulted in a decrease in nitrogen C_d . This result also differs from the hot firing case. Evidently, the effects of tube recess and extension on both C_d and stability are combustion related.

A possible explanation is offered for this difference in behavior between the cold flow and hot firing tests. In the cold flow case, it could be that some of the gas (nitrogen) emerging through the annulus is entrained into the liquid (water) stream. This ejection by the oxygen stream, which is relatively undisturbed in the recess cavity, would reduce the hydrogen injection pressure drop (an apparent increase in C_d). In the hot firing case, this effect appears to be counteracted by some stronger effect. It may be that the heat from the injector element walls (and/or faceplate) warms and expands the hydrogen gas in the recess cavity, thus reducing the density and increasing injection pressure drop producing an apparent decrease in C_d .

The 157 element data were much like the 421 element injector. Recessing the oxidizer tubes approximately two diameters improved combustion performance (fig. 9(d)). Contrary to the 421 element results, however, the performance remained constant as the recess was further increased.

Going the other way to tube extension, there was an initial step increase in ηC^* from 93 percent for the flush tubes to 97 percent for a 0.635-centimeter (0.25-in.) extension. Performance then showed a slight decrease with further extension to 1.904 centimeters (0.75 in.). However, as the tubes were extended to 3.18 centimeters (1.25 in.) (stable point), there was a significant drop in ηC^* (about 8 percent). This decrease in performance may be the result of two combined effects - the tube extension and the lower hydrogen injection temperature. Reference 12 indicated that combustion performance generally decreases with decreasing fuel temperatures for hydrogen oxygen engines. Although data are not available at higher hydrogen injection temperatures, performance would be expected to be higher than the value reported in figure 9(d) corresponding to the cold transition temperature.

Thus, the overall characteristics of the engine using an extended tube injector indicate that there is no value of tube extension that could be used to advantage.

Effect of Element Tube Concentricity

The question has frequently been posed as to the effect of manufacturing inaccuracies on combustion stability, particularly with fine injector elements. With concentric tube injectors, the question of oxidizer tube concentricity within the hydrogen annuli was

of particular interest owing to the elaborate machine work required to ensure that the tubes would initially be concentric and remain so during firing. To supply a gross answer to this question, two injectors were constructed which were identical except for spacers used to force concentricity in one injector (fig. 4(e)). Significant random eccentricity in manufacture was present in the other injector (fig. 4(f)).

Results in terms of screech limit and performance are given in figure 10. It is seen in figure 10(b) that hydrogen C_d for the concentric elements are lower than those for the random case. This was probably caused by a slight, unavoidable obstruction created by the presence of the concentricity assurance washers (see fig. 4(g)). Since lower C_d 's mean higher injector pressure drops which, in turn, produce greater stability, it would be expected that figure 10(a) would show greater stability for the more concentric elements. However, within the precision of the test techniques, it is difficult to discern any appreciable effect of concentricity on stability from figure 10(a). This configuration series, therefore, produced data slightly anomalous to the correlation of C_d changes with stability.

Figure 10(c) also shows no appreciable effect of assured concentricity on performance. Accordingly, there is insufficient evidence to justify extreme measures to ensure precise concentricity of straight tube concentric elements with gaseous hydrogen liquid oxygen propellants.

Discharge Coefficient as a Correlation Parameter

The implication of the present data has been that for the same injection area ratio and thrust per element, changes in element detail produce changes in fuel flow coefficients which result in an alteration of the high-frequency stability limits. In figure 11, the data from all tests (except oxidizer tube extension) are presented in terms of fuel injection pressure drop and fuel injection temperature at transition to instability. The two stable tests are also shown at the lowest temperature tested.

The 421 element series indicates that the changes in element detail (oxidizer tube recess series) produced adjustments in the pressure-temperature schedule (via changes in C_d) in such a way that all three transitions occurred at about the same fuel injection ΔP but at quite different fuel injection temperatures. At the lowest temperature possible for testing, the ΔP was well above the minimum for stability with 1.27 centimeters (0.5 in.) recess.

The 157 element data do not indicate this same critical ΔP characteristic quite as clearly. The injection angle and oxidizer tube recess data are within ± 10 percent of a constant value of $406\,790.67\text{ N/m}^2$ (59 psi) for fuel injection ΔP . The blunt oxidizer tube and the concentricity assurance washer configurations fall outside of this band and, consequently, are not presented. But as mentioned in earlier sections, the stability of

these configurations did not correlate well with simply hydraulic considerations. The ΔP for the stable 157 element point was well above the critical value at the lowest temperature possible for testing.

Modified Definition of Injection Area Ratio as a Correlating Parameter

Direct comparison of two sets of data with 15⁰, 421 element injectors is now possible. In reference 4, hydrogen-to-oxygen injection area ratio changes were made by physically changing the injection areas while in the present results, effective area ratio changes were made by changing only the element details. Both the present data and those of reference 4 indicate that decreasing effective injection area ratio (computed using measured areas multiplied by C_d 's) improves stability. The flush configurations from reference 4 may be superimposed on the present data by applying a discharge coefficient to fuel injection area. Even after modifying the definition of area, the recessed points do not precisely fit the reference 4 correlation indicating that the effect of recess on stability may not be completely described as a change in effective flow area.

Correlation with Response Factor Model

In seeking to explain the experimental results, the data were examined for concurrence with a response-factor model proposed in reference 3. It was shown that for certain values of flow resistance (injector pressure drop), the hydrogen flow rate can respond to high-frequency pressure oscillations in the combustor, thus providing a coupling which can drive screech much like the accepted mechanism for chugging. The model envisions a series of weighted response factors which may be either driving or damping. Positive factors are driving and negative factors are damping. Neutral stability occurs when the summation of all response factors is zero. For simplicity in the analysis, only three terms are considered; response of the hydrogen, response of the oxygen, and response of the exhaust nozzle. In using the response model to correlate the present data, both oxygen and nozzle response have been assumed to be insensitive to the hardware and engine parameters varied in this program. Support for this assumption can be found in references 13 and 14. Therefore, by evaluating the hydrogen response factor for each configuration, stability may be inferred.

Hydrogen response factor is plotted in figure 12 as a function of hydrogen density (and temperature) for the series of tests where impingement angle was varied. Four curves are shown in figure 12, one for each impingement angle. These curves were derived analytically from equations (20), (24), and (25) in reference 3 using the

constants listed in table IV. The effect of impingement angle is accommodated in the response model by redefining the flow area term. Instead of using the measured area A_{meas} an effective area A_{eff} was determined using the discharge coefficients presented earlier where

$$A_{\text{eff}} = C_d \times A_{\text{meas}}$$

The effective areas are keyed with the symbols on figure 12. When the symbols are superimposed upon their respective curves at the measured hydrogen transition temperature, it is seen that an almost constant value of response factor of about 0.9 is indicated. The constant value of hydrogen response factor is consistent with the assumption that the other system responses (i. e. , oxygen and nozzle) are insensitive to the injection element variables investigated.

It is interesting to look at these curves in light of the mode of operation, that is, ramping hydrogen temperature downwards or density upwards through the screech limit. Starting at the left of the zero angle curve of figure 12, for example, it is seen that as we move to the right (density ramp upwards), we get increasing positive values of response factor until we reach the value of 0.9 at the transition density. For this configuration, a response factor above 0.9 represents instability. Since higher densities produce lower injection pressure drops (flow resistance), the relation between low pressure drop and instability is seen. Referring to figure 12, it appears that increasing impingement angle from 0° to 45° decreases the effective flow area of the hydrogen annulus and increases the flow resistance which results in greater stability.

In a similar fashion, the effects of recessing on the 157 element injector are illustrated in figure 13. The three transition points occur at about the same level of response factor (0.8 to 1.0). The maximum recess configuration never reached this required level and accordingly did not screech. Here again, the mechanism appears to be a reduction in effective area (due to the recess in this case) with a concomitant change in element flow resistance. These data again seem consistent with the response factor model. No attempt was made to correlate the data on tube extension because the constant C_d indicated for the five different extensions make the response model insensitive to these configuration changes.

The effects of varying the oxidizer tube base thickness of the coarse element injector is illustrated in figure 14. The three transition points are shown to occur within the range 0.9 to 1.2.

Finally, the data on tube recess with the 421 fine elements was examined in the same way, and results are given in figure 15. Here, the required response factor for screech was again constant around 1.1. At maximum recess of 1.27 centimeters (0.5 in.), stability is predicted by the model and verified experimentally.

As mentioned previously, fuel injection ΔP as a correlating parameter seemed to be useful for a particular thrust per element but was not useful in predicting the stability with a previously untested element size. Similarly, the injection area ratio correlation has inherently the same problem even though it has the added advantage of doing a fair job of predicting stability for both real and effective fuel injection area changes. Presented in figure 16 are the fuel system response values for all the present data, except the oxidizer tube extension, superimposed on a single plot at the respective transition densities. Data representing a thrust-per-element range of from 22.7 to 59 kilograms (50 to 130 lb), injection angles of from 0° to 45° , oxidizer tube recess up to 1.27 centimeters (0.5 in.), oxidizer tube base thickness from 0.0349 to 0.173 centimeter (0.01375 to 0.06800 in.) and elements with random concentricity and with assured concentricity are correlated with a single value of fuel system response factor of 1.0 ± 20 percent with the two stable configurations being well outside of the band of unstable points. Assuming similar values of response for other systems (i. e., oxidizer, nozzle, friction, aerodynamics, etc.), the stability of a hydrogen-oxygen engine should be, therefore, predictable.

SUMMARY OF RESULTS

An experimental investigation was conducted at the Lewis Research Center to learn more about how the specific details of a concentric tube injection element affect the screech characteristics of a hydrogen-oxygen rocket engine. The four variables investigated were (1) impingement angle, (2) oxidizer tube blunt base thickness, (3) oxidizer tube recess and extension, and (4) oxidizer tube-annulus concentricity. Tests were made using a 27.34-centimeter- (10.77-in.) diameter heat-sink combustor at nominally 206×10^6 -N/m² (300-psia) chamber pressure. All of the test variables were investigated using a 157 element circular pattern injector. Additional oxidizer tube recess tests were made with a 421 element hexagonal pattern injector. Tests were conducted over the oxidant-fuel ratio range of 4 to 6. Stability evaluation for each configuration was made using the hydrogen temperature rating technique. Several element configurations were also cold flow tested using nitrogen and water as simulants. For these configurations, the following results were obtained:

1. By use of the response factor model of NASA TN D-4040, the long observed effect of hydrogen temperature on screech limits of hydrogen-oxygen rockets is explained as being due to the change in injector hydrogen flow resistance. And, further, this model can be used to correlate data from a range of thrust-per-element tests using several different types of injection elements.

2. Similarly, changes in stability due to changes in injection velocity ratio are also explainable through the mechanism of changes in injector hydrogen flow resistance.

3. As the impingement angle of concentric tube injectors was increased from 0° (parallel flow) to 45° , stability was improved with no effect on performance.

4. The data for oxidizer tube blunt base thickness effect indicate a critical thickness which corresponds to minimum stability but the necessary changes in the hydrogen flow passages may also have affected the results.

5. Recessing of the oxidizer tubes improved stability continuously with depth until completely stable configurations were achieved (with elements of two different sizes). Efficiency also improved with recess up to approximately two oxidizer tube diameters.

6. Progressive extension of the oxidizer tubes into the thrust chamber decreased stability until a discontinuity occurred. Beyond the discontinuity, operation was completely stable but efficiency was markedly reduced.

7. No significant effect of oxidizer tube-annulus concentricity was found on either stability or performance.

Lewis Research Center,
National Aeronautics and Space Administration,
Cleveland, Ohio,
502-24.

REFERENCES

1. Dankhoff, Walter F.; Johnsen, Irving A.; Conrad, E. William; and Tomazic, William A.: M-1 Injector Development-Philosophy and Implementation. NASA TN D-4730, 1968.
2. Conrad, E. William; Bloomer, Harry E.; Wanhainen, John P.; and Vincent, David W.: Interim Summary of Liquid Rocket Acoustic-Mode-Instability Studies at a Nominal Thrust of 20,000 Pounds. NASA TN D-4968, 1968.
3. Feiler, Charles E.; and Heidmann, Marcus F.: Dynamic Response of Gaseous-Hydrogen Flow Systems and its Application to High-Frequency Combustion Instability. NASA TN D-4040, 1967.
4. Wanhainen, John P.; Parish, Harold C.; and Conrad, E. William: Effect of Propellant Injection Velocity on Screech in a 20,000-Pound Thrust Hydrogen-Oxygen Rocket. NASA TN D-3373, 1966.
5. Ladd, J. W.: A Durable and Reliable Test Stand System for High-Accuracy Temperature Measurements in the Cryogenic Ranges of Liquid Hydrogen and Liquid Oxygen. Advances in Cryogenic Engineering. Vol. 6. K. D. Timmerhaus, ed., Plenum Press, 1961, pp. 388-395.

6. Herr, Austin C.; Terbeek, Howard G.; and Tieferman, Marvin W.: Suitability of Carbon Resistors for Field Measurements of Temperatures in the Range 35⁰ to 100⁰ R. NASA TN D-264, 1960.
7. Huff, Vearl N.; Fortini, Anthony; and Gordon, Sanford: Theoretical Performance of JP-4 Fuel and Liquid Oxygen as a Rocket Fuel. II - Equilibrium Composition. NACA RM E56D23, 1956.
8. Gordon, Sanford; and McBride, Bonnie J.: Theoretical Performance of Liquid Hydrogen with Liquid Oxygen as a Rocket Propellant. NASA Memo 5-21-59E, 1959.
9. Anon.: An Experimental Investigation of Combustion Stability Characteristics of Liquid Oxygen-Liquid Hydrogen at High Chamber Pressure. Rep. 11741, Aerojet-General Corp. (NASA CR-78691), Aug. 25, 1966.
10. Anon.: Flow of Fluids. Tech. Paper No. 410, Crane Co., 1957.
11. Wanhainen, John P.; Hannum, Ned P.; and Russell, Louis M.: Evaluation of Screech Suppression Concepts in a 20,000-Pound Thrust-Hydrogen-Oxygen Rocket. NASA TM X-1435, 1967.
12. Salmi, Reino J.; Wanhainen, John P.; and Hannum, Ned P.: Effect of Thrust per Element on Combustion Stability Characteristics of Hydrogen-Oxygen Rocket Engines. NASA TN D-4851, 1968.
13. Heidmann, Marcus F.; and Wieber, Paul R.: Analysis of Frequency Response Characteristics of Propellant Vaporization. NASA TN D-3749, 1966.
14. Crocco, Luigi; and Sirignano, William A.: Behavior of Supercritical Nozzles Under Three-Dimensional Oscillatory Conditions. AGARDograph 117, 1967.
15. Wanhainen, John P.; Feiler, Charles E.; and Morgan, C. Joe: Effect of Chamber Pressure, Flow Per Element, and Contraction Ratio on Acoustic-Mode Instability in Hydrogen-Oxygen Rockets. NASA TN D-4733, 1968.

TABLE I. - EXPERIMENTAL DATA

Configuration	Test	Hydrogen injection temperature		Hydrogen injection density		Chamber pressure		Oxidant-fuel ratio, O/F	Oxygen weight flow		Hydrogen weight flow		Oxygen injector pressure drop		Hydrogen injector pressure drop		Oxygen injector flow coefficient, $(C_d)_{O_2}$	Hydrogen injector flow coefficient, $(C_d)_{H_2}$	Characteristic exhaust velocity efficiency, ηC^* , percent	Stability classification
		K	°R	kg/m ³	lb/ft ³	N/m ²	psi		kg/sec	lb/sec	kg/sec	lb/sec	N/m ²	psi	N/m ²	psi				
		Oxidizer tube recess and extension studies - 157 element																		
0.064-cm (0.025-in.) extension	571	63.9	115	8.01	0.50	1.986×10 ⁶	288	6.01	23.6	52.1	3.93	8.66	3.875×10 ⁶	562	2.930×10 ⁵	42.5	0.774	0.976	92.9	Transition ↓
	572	61.7	111	7.69	.48	1.917	278	5.14	22.7	50.0	4.41	9.73	3.516	510	3.751	54.4	.780	.989	90.3	
	573	56.7	102	10.25	.64	2.096	304	3.98	21.7	47.9	5.49	12.10	3.275	475	4.385	63.6	.774	.985	95.5	
	574	69.4	125	7.37	.46	2.027	294	4.46	22.7	50.0	5.08	11.20	3.282	476	4.764	69.1	.807	1.032	91.3	
	575	69.4	116	8.01	.50	1.979	287	5.50	23.3	51.3	4.23	9.33	3.778	548	3.578	51.9	.772	.952	93.1	
0.635-cm (0.25-in.) extension	921	61.7	111	9.61	0.60	2.241×10 ⁶	325	5.42	24.3	53.6	4.48	9.88	4.054×10 ⁶	588	3.84×10 ⁵	55.7	0.779	0.888	99.5	Transition ↓
	922	58.3	105	10.09	.63	2.186	317	4.17	22.2	48.9	5.31	11.71	3.351	486	5.026	72.9	.781	.898	98.2	
	924	61.1	110	9.41	.59	2.165	314	6.10	25.9	57.1	4.24	9.35	4.426	642	3.468	50.3	.794	.892	95.1	
1.27-cm (0.50-in.) extension	906	80.0	144	6.25	0.39	2.034×10 ⁶	295	4.73	22.0	48.6	4.67	10.3	-----	---	5.171×10 ⁵	75.0	-----	0.989	96.0	Transition ↓ Stable Transition ↓
	907	70.5	127	7.85	.49	2.117	307	4.09	21.7	47.8	5.31	11.7	3.420×10 ⁶	496	6.502	94.3	0.756	.894	97.6	
	908	88.3	159	6.09	.38	2.186	317	6.69	25.7	56.7	3.85	8.5	4.489	651	4.358	63.2	.783	.901	99.7	
	909	70.5	127	7.69	.48	2.117	307	6.68	26.0	57.3	3.90	8.6	4.668	677	3.627	52.6	.776	.889	95.4	
	910	73.3	132	7.53	.47	2.172	315	4.60	22.6	49.8	4.90	10.8	3.503	508	5.226	75.8	.778	.940	99.3	
	911	83.3	150	6.41	.40	2.186	317	5.99	25.0	55.1	4.17	9.2	4.220	612	4.723	68.5	.784	.913	98.6	
	912	70.5	127	7.69	.48	2.137	310	5.35	24.1	53.2	4.54	10.0	-----	---	5.192	75.3	-----	.864	95.8	
1.904-cm (0.75-in.) extension	888	71.1	128	7.37	0.46	-----	---	4.69	25.8	56.8	5.12	11.3	4.254×10 ⁶	617	5.185×10 ⁵	75.2	0.805	0.998	-----	Unstable Transition ↓
	889	83.9	151	6.09	.38	2.068×10 ⁶	300	4.93	23.4	51.7	4.76	10.5	4.137	600	4.689	68.0	.743	1.073	93.3	
	890	73.3	132	7.05	.44	2.179	316	3.94	23.6	52.1	5.53	12.2	3.503	508	6.902	100.1	.814	.956	98.7	
	891	80.5	145	6.41	.40	2.068	300	6.40	24.8	54.8	3.90	8.6	4.489	651	3.958	57.4	.756	.932	96.3	
	892	76.7	138	6.73	.42	2.117	307	4.57	23.5	51.9	4.90	10.8	3.489	506	6.888	99.9	.813	1.170	97.3	
3.18-cm (1.25-in.) extension	876	30.0	54	60.23	3.76	2.144×10 ⁶	311	5.23	25.8	56.9	4.94	10.9	4.923×10 ⁶	714	0.703×10 ⁵	10.2	0.750	0.914	89.0	Stable ↓
	877	30.5	54	58.79	3.67	2.165	314	3.99	24.8	54.8	6.21	13.7	4.385	636	1.875	22.2	.765	.718	85.9	
	878	32.2	58	55.43	3.46	2.110	306	6.55	27.0	59.6	4.13	9.1	5.102	740	1.289	18.7	.772	.588	90.85	

TABLE I. - Continued. EXPERIMENTAL DATA

Configuration	Test	Hydrogen injection temperature		Hydrogen injection density		Chamber pressure		Oxidant-fuel ratio, O/F	Oxygen weight flow		Hydrogen weight flow		Oxygen injector pressure drop		Hydrogen injector pressure drop		Oxygen injector flow coefficient, $(C_d)_{O_2}$	Hydrogen injector flow coefficient, $(C_d)_{H_2}$	Characteristic exhaust velocity efficiency, η_{C^*} , percent	Stability classification
		K	$^{\circ}R$	kg/m ³	lb/ft ³	N/m ²	psi		kg/sec	lb/sec	kg/sec	lb/sec	N/m ²	psi	N/m ²	psi				
		Oxidizer tube recess and extension studies - 157 element																		
0.254-cm (0.10-in.) recess	674	55.0	99	10.57	0.66	2.103 $\times 10^6$	305	5.17	23.6	52.0	4.57	10.07	3.447 $\times 10^6$	500	4.330 $\times 10^5$	62.8	0.819	0.812	95.8	Transition ↓
	675	51.0	92	12.82	.80	2.179	316	3.97	22.0	48.5	5.54	12.22	2.985	433	5.095	73.9	.821	.825	98.3	
	676	55.0	99	10.25	.64	2.041	296	6.42	24.7	54.5	3.85	8.49	3.799	551	3.303	47.9	.818	.796	95.6	
	677	52.8	95	11.37	.71	2.103	305	4.53	22.6	49.8	4.99	11.01	3.103	450	4.944	71.7	.827	.802	95.9	
	678	52.8	95	11.21	.70	2.068	300	5.64	24.1	53.2	4.28	9.44	3.461	502	3.765	54.6	.836	.793	94.9	
0.508-cm (0.20-in.) recess	695	50.0	90	11.05	0.69	1.848 $\times 10^6$	268	5.36	22.2	48.9	4.14	9.12	4.054 $\times 10^6$	588	3.503 $\times 10^5$	50.8	0.710	0.800	93.6	Transition ↓
	696	45.5	82	14.90	.93	2.062	299	4.13	22.6	49.8	5.46	12.04	4.171	605	4.027	58.4	.713	.849	94.6	
	697	46.7	84	13.62	.85	1.972	286	6.11	24.9	55.0	4.09	9.01	5.206	755	3.199	46.4	.705	.745	92.9	
	698	48.9	88	13.30	.83	2.068	300	4.64	23.4	51.5	5.03	11.09	4.426	642	4.302	62.4	.716	.800	94.8	
	699	53.3	96	11.05	.69	2.041	296	5.61	24.4	53.8	4.35	9.60	4.916	713	4.371	63.4	.710	.754	95.1	
	700	50.5	91	11.85	.74	1.999	290	6.22	25.2	55.5	4.04	8.91	5.226	758	3.303	47.9	.710	.777	94.0	
0.84-cm (0.33-in.) recess	721	33.3	60	50.78	3.17	1.820 $\times 10^6$	264	5.33	21.3	46.9	3.99	8.80	5.668 $\times 10^6$	822	6.943 $\times 10^5$	100.7	0.576	0.256	96.1	Stable ↓
	722	30.5	55	59.11	3.69	2.075	301	4.12	22.4	49.3	5.43	11.97	6.040	876	7.205	104.5	.587	.317	96.5	
	723	31.1	56	57.03	3.56	1.937	281	6.19	24.1	53.1	3.89	8.58	6.647	964	4.420	64.1	.602	.295	95.1	
Oxidizer tube concentricity studies - 157 element																				
With concentricity washers	682	65.5	118	8.01	0.50	2.055 $\times 10^6$	298	5.01	22.5	49.6	4.49	9.69	3.696 $\times 10^6$	536	5.633 $\times 10^5$	81.7	0.755	0.804	97.4	Transition ↓
	683	64.4	116	8.01	.50	2.020	293	5.03	22.4	49.5	4.46	9.85	3.696	536	5.295	76.8	.753	.824	95.9	
	684	65.5	118	8.17	.51	2.062	299	4.97	22.7	50.0	4.56	10.65	3.834	556	5.543	80.4	.747	.814	96.7	
	685	57.8	104	9.29	.58	2.006	291	5.92	23.9	52.8	4.05	8.93	4.171	605	3.744	54.3	.756	.827	94.5	
	686	51.1	92	11.85	.74	2.082	302	4.04	21.9	46.3	5.42	11.96	3.544	514	4.964	72.0	.750	.850	95.1	

TABLE I. - Continued. EXPERIMENTAL DATA

Configuration	Test	Hydrogen injection temperature		Hydrogen injection density		Chamber pressure		Oxidant-fuel ratio, O/F ¹	Oxygen weight flow		Hydrogen weight flow		Oxygen injector pressure drop		Hydrogen injector pressure drop		Oxygen injector flow coefficient, (C _d) _{O₂}	Hydrogen injector flow coefficient, (C _d) _{H₂}	Characteristic exhaust velocity efficiency, ηC*, percent	Stability classification
		K	°R	kg/m ³	lb/ft ³	N/m ²	psi		kg/sec	lb/sec	kg/sec	lb/sec	N/m ²	psi	N/m ²	psi				
Injection angle studies - 157 element																				
45° impingement angle	583	48.9	88	13.14	0.82	2.144×10 ⁶	311	4.83	24.2	53.4	5.02	11.07	4.192×10 ⁶	608	4.399×10 ⁵	63.8	0.763	0.795	93.7	Transition ↓
	584	42.2	76	18.10	1.13	2.130	309	3.78	22.6	49.8	5.98	13.18	3.668	532	4.489	65.1	.760	.799	93.3	
	585	49.4	89	12.49	.78	2.089	303	5.88	24.5	54.0	4.17	9.19	4.868	706	3.254	47.2	.716	.787	96.7	
	586	45.0	81	15.70	.98	2.137	310	4.27	23.3	51.3	5.43	11.98	4.047	587	4.323	62.7	.746	.794	93.9	
	587	43.9	79	15.70	.98	2.089	303	5.98	25.0	55.1	4.17	9.20	5.502	798	2.613	37.9	.687	.784	95.3	
30° impingement angle	853	53.3	96	10.25	0.64	1.972×10 ⁶	286	4.87	22.0	48.5	4.51	9.95	-----	---	4.578×10 ⁵	66.4	-----	0.793	94.4	Transition ↓
	856	40.0	72	20.50	1.28	2.068	300	3.94	22.3	49.2	5.66	12.48	-----	---	3.151	45.7	-----	.848	91.4	
	857	40.0	72	20.83	1.30	2.096	304	3.94	22.5	49.7	5.72	12.62	-----	---	3.089	44.8	-----	.859	91.9	
	858	56.1	101	9.93	.62	2.034	295	5.96	24.1	53.1	4.05	8.92	-----	---	4.006	58.1	-----	.772	95.6	
15° impingement angle	514	61.1	110	9.77	0.61	2.062×10 ⁶	299	4.82	22.5	49.7	4.68	10.31	3.337×10 ⁶	484	6.895×10 ⁵	100.0	0.796	0.686	95.1	Stable Transition Stable Transition ↓
	515	53.9	97	11.05	.69	2.124	308	3.86	21.2	46.8	5.50	12.12	3.165	459	4.716	68.4	.769	.916	97.6	
	516	71.1	128	9.13	.57	2.068	300	5.37	23.5	51.8	4.39	9.67	3.992	579	4.978	72.2	.758	.783	98.5	
	517	58.3	105	8.97	.56	1.965	285	6.01	23.4	51.7	3.90	8.60	3.909	567	2.889	41.9	.765	.922	94.1	
	518	62.8	113	8.33	.52	2.006	291	5.37	22.7	50.1	4.22	8.31	3.985	528	3.827	55.5	.768	.900	95.6	
	519	60.0	108	8.33	.52	1.999	290	5.03	22.2	49.0	4.42	9.74	3.482	555	3.965	57.5	.768	.925	95.2	
0° impingement angle	576	65.5	118	8.01	0.50	2.020×10 ⁶	293	4.84	22.7	50.0	4.69	10.35	3.572×10 ⁶	518	4.137×10 ⁵	60.0	0.774	0.980	94.7	Transition ↓
	577	48.3	87	13.62	.85	2.151	312	3.90	22.5	49.6	5.93	13.07	3.413	495	3.841	55.7	.785	.987	94.7	
	578	70.5	127	7.53	.47	2.110	306	5.66	24.9	54.9	4.39	9.69	4.344	630	3.399	49.3	.770	1.045	95.0	
	582	68.3	123	7.21	.45	-----	---	6.02	25.6	56.4	4.25	9.37	4.937	716	4.944	71.7	.742	.858	---	

TABLE I. - Concluded. EXPERIMENTAL DATA

Configuration	Test	Hydrogen injection temperature		Hydrogen injection density		Chamber pressure		Oxidant-fuel ratio, O/F	Oxygen weight flow		Hydrogen weight flow		Oxygen injector pressure drop		Hydrogen injector pressure drop		Oxygen injector flow coefficient, $(C_d)_{O_2}$	Hydrogen injector flow coefficient, $(C_d)_{H_2}$	Characteristic exhaust velocity efficiency, η_{C^*} , percent	Stability classification
		K	$^{\circ}R$	kg/m ³	lb/ft ³	N/m ²	psi		kg/sec	lb/sec	kg/sec	lb/sec	N/m ²	psi	N/m ²	psi				
Oxidizer tube base thickness studies - 157 element																				
0.173-cm (0.06800-in.) blunt base	688	51.7	93	11.69	0.73	2.089×10 ⁶	303	5.09	23.4	51.6	4.59	10.13	4.040×10 ⁶	586	2.813×10 ⁵	40.8	0.751	0.964	95.5	Transition ↓
	689	43.9	79	16.02	1.00	2.124	308	4.08	22.2	48.9	5.44	12.00	3.578	519	2.661	38.6	.756	1.003	95.5	
	690	58.9	106	8.81	.55	1.972	286	6.23	23.7	52.2	3.80	8.38	4.261	618	2.723	39.5	.739	.933	95.5	
	691	51.1	92	11.53	.72	2.089	303	4.64	22.5	49.6	4.84	10.67	3.689	535	3.978	57.7	.755	.860	96.2	
	692	56.7	102	9.45	.59	1.999	290	5.73	23.5	51.8	4.10	9.04	4.047	587	2.551	37.0	.753	1.052	94.8	
0.349-cm (0.01375-in.) blunt base	693	61.7	111	8.65	0.54	2.103×10 ⁶	305	5.01	23.0	50.8	4.60	10.14	3.916×10 ⁶	568	3.847×10 ⁵	55.8	0.751	0.960	97.2	Stable Transition ↓
	894	54.4	98	10.09	.63	1.986	288	5.78	23.8	52.5	4.11	9.07	5.123	743	3.047	44.2	.678	.893	93.0	
	895	46.7	84	14.42	.90	2.165	314	4.21	22.8	50.3	5.42	11.95	4.247	616	3.482	50.5	.714	.921	95.4	
	897	62.2	112	9.29	.58	2.186	317	5.32	24.1	53.1	4.53	9.98	4.957	719	4.447	64.5	.697	.848	98.2	
	898	52.8	95	11.37	.71	2.137	310	4.84	23.1	50.9	4.77	10.52	4.316	626	3.882	56.3	.716	.864	97.1	
Oxidizer tube recess studies - 421 element																				
1.27-cm (0.50-in.) recess	567	35.0	63	43.25	2.7	2.110×10 ⁶	306	4.43	23.6	52.0	5.32	11.73	1.813×10 ⁶	263	5.833×10 ⁵	84.6	0.617	0.254	90.2	Stable ↓
	568	29.4	53	62.48	3.9	2.068	300	3.54	22.2	48.8	6.27	13.82	1.986	288	-----	-----	.554	-----	87.9	
	569	30.5	55	59.27	3.7	2.027	294	6.17	25.2	55.5	4.07	8.98	1.793	260	3.978	57.7	.662	.199	90.5	
	570	30.0	54	60.88	3.8	2.082	302	4.53	23.4	51.7	5.17	11.42	1.779	258	6.419	93.1	.619	.197	86.9	
0.762-cm (0.30-in.) recess	589	38.3	69	25.31	1.58	2.137×10 ⁶	310	4.51	23.2	51.1	5.07	11.18	1.462×10 ⁶	212	2.820×10 ⁵	40.9	0.675	0.451	94.5	Transition ↓
	590	38.9	70	23.71	1.48	2.144	311	5.58	24.9	54.9	4.46	9.84	1.682	244	2.351	34.1	.676	.449	94.0	
	591	38.9	70	23.55	1.47	2.089	303	4.49	24.5	51.0	5.14	11.33	1.489	216	3.151	45.7	.667	.448	92.1	
	592	37.8	68	27.55	1.72	2.158	313	3.90	22.2	48.9	5.68	12.52	1.317	191	2.730	39.6	.680	.492	95.3	

TABLE II. - CROSS PLOT DATA

[Oxidant-fuel ratio, 5.0; hydrogen flow rate, 4.67 kg/sec (10.3 lb/sec); oxygen flow rate, 23.4 kg/sec (51.5 lb/sec).]

Configuration	Hydrogen injection temperature		Hydrogen injection density		Characteristic exhaust velocity efficiency, η_{C^*} , percent	Hydrogen injector pressure drop		Hydrogen injector flow coefficient, $(C_d)_{H_2}$	Oxygen injector pressure drop		Oxygen injector flow coefficient, $(C_d)_{O_2}$	Stability classification
	K	$^{\circ}R$	kg/m ³	lb/ft ³		N/m ²	psi		N/m ²	psi		
Oxidizer tube recess and extension studies - 157 element												
0.064-cm (0.025-in.) extension	61.1	110	8.95	0.559	92.5	4.137×10 ⁵	60.0	0.987	3.806×10 ⁶	552	0.781	Transition
0.635-cm (0.25-in.) extension	60.0	108	9.18	.573	97.3	4.033	58.5	.893	↓	↓	.781	↓
1.27-cm (0.50-in.) extension	74.4	134	6.98	.436	97.1	5.295	76.8	.915	↓	↓	.775	↓
1.904-cm (0.75-in.) extension	78.9	142	6.54	.408	95.7	5.668	82.2	1.033	↓	↓	.786	↓
3.18-cm (1.25-in.) extension	30.5	55	58.95	3.68	88.8	.627	9.1	.740	↓	↓	.762	Stable
0.254-cm (0.10-in.) recess	53.3	96	10.89	.680	96.5	4.468	64.8	.806	3.344	485	.824	Transition
0.508-cm (0.20-in.) recess	48.3	87	12.82	.800	94.5	3.978	57.7	.788	4.551	660	.711	Transition
0.84-cm (0.33-in.) recess	31.7	57	56.39	3.52	96.2	6.467	93.8	.289	6.840	992	.588	Stable
Oxidizer tube concentricity studies - 157 element												
With concentricity washers	583	105	9.55	0.596	96.0	5.185×10 ⁵	75.2	0.824	3.930×10 ⁶	570	0.752	Transition
Injection angle studies - 157 element												
45 ^o impingement angle	46.1	83	14.05	0.877	94.7	3.640×10 ⁵	52.8	0.792	3.999×10 ⁶	580	0.734	Transition
30 ^o impingement angle	51.1	92	11.66	.728	93.5	4.220	61.2	.818	-----	---	-----	↓
15 ^o impingement angle	58.3	105	9.55	.596	96.0	3.992	57.9	.916	3.861	560	.771	↓
0 ^o impingement angle	62.8	113	8.68	.542	94.7	3.909	56.7	.968	3.792	550	.768	↓
Oxidizer tube base thickness studies - 157 element												
0.173-cm (0.06800-in.) blunt base	51.7	93	11.45	0.715	95.3	3.082×10 ⁵	44.7	0.962	4.068×10 ⁶	590	0.751	Transition
0.349-cm (0.01375-in.) blunt base	53.9	97	10.68	.667	96.0	3.723	54.0	.897	4.413	640	.711	Transition
Oxidizer tube recess studies - 421 element												
1.27-cm (0.50-in.) recess	30.5	55	58.95	3.68	89.5	-----	---	0.216	-----	---	0.613	Stable
0.762-cm (0.30-in.) recess	38.9	70	22.59	1.41	94.2	2.883×10 ⁵	41.8	.460	1.448×10 ⁶	210	.674	Transition
0.238-cm (0.094-in.) recess ^a	43.3	78	16.18	1.01	99.0	2.572	37.3	.516	1.358	197	.704	↓
Flush ^b	73.3	132	7.05	.44	97.0	2.586	37.5	.886	1.262	183	.805	↓

^aData from ref. 4, p. 13.

^bData from ref. 15.

TABLE III. - COLD FLOW DATA
 [Chamber pressure, 13.79×10^6 N/m² (200 psi).]

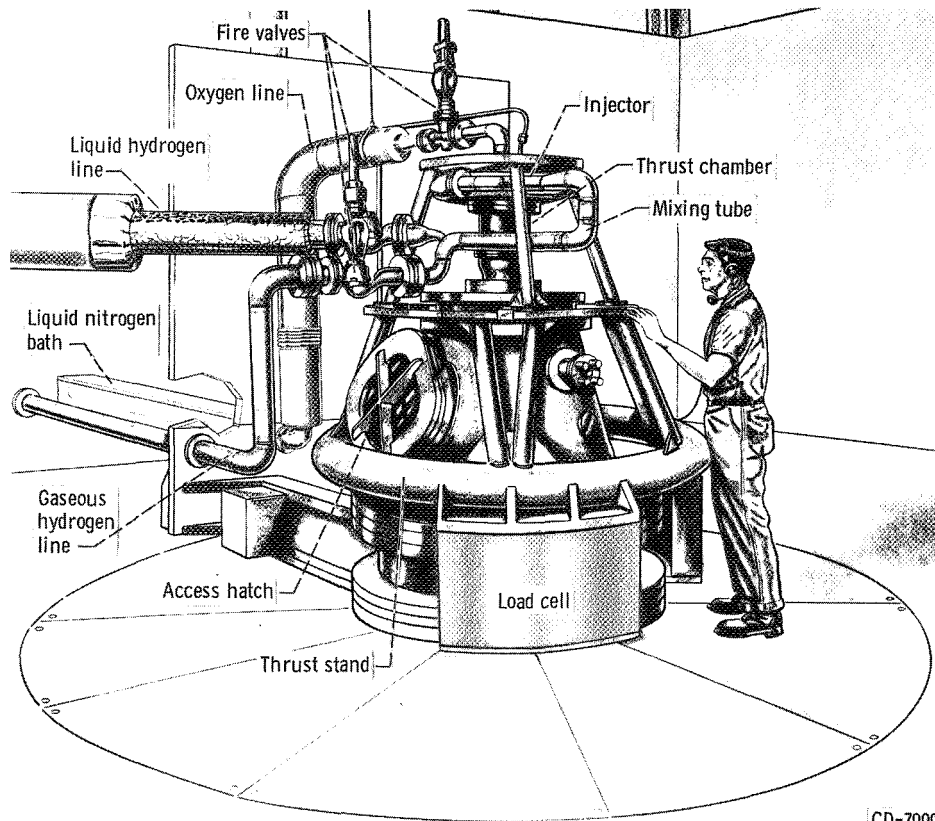
Configuration	Nitrogen flow rate		Nitrogen pressure drop		$(C_d)_N$ based on flow of 27.25 g/sec (0.06 lb/sec)	H ₂ O flow rate		H ₂ O pressure drop		$(C_d)_{H_2O}$
	kg/sec	lb/sec	N/m ²	psi		kg/sec	lb/sec	N/m ²	psi	
Recess and extension										
Standard, flush	0.0202	0.0446	0.938×10^5	13.6	1.020	0.1089	0.24	2.199×10^6	319	0.845
	.0267	.0589	1.565	22.7	↓	↓	↓	↓	↓	↓
	.0350	.0772	2.441	35.4	↓	↓	↓	↓	↓	↓
	.0414	.0914	3.385	49.1	↓	↓	↓	↓	↓	↓
	.0357	.0788	2.606	37.8	↓	↓	↓	↓	↓	↓
0.254-cm (0.10-in.) recess	0.0210	0.0464	0.786×10^5	11.4	1.140	0.1089	0.24	1.965×10^6	285	0.894
	.0281	.0620	1.372	19.9	↓	↓	↓	↓	↓	↓
	.0328	.0723	1.813	26.3	↓	↓	↓	↓	↓	↓
0.508-cm (0.20-in.) recess	0.0220	0.0485	0.862×10^5	12.5	1.162	0.1043	0.23	-----	---	---
	.0339	.0747	1.400	20.3	↓	↓	↓	↓	↓	↓
	.0356	.0786	2.048	29.7	↓	↓	↓	↓	↓	↓
	.0426	.0940	2.799	40.6	↓	↓	↓	↓	↓	↓
0.84-cm (0.33-in.) recess	0.0227	0.0500	0.876×10^5	12.7	1.162	0.1043	0.23	1.999×10^6	290	0.849
	.0274	.0604	1.241	18.0	↓	↓	↓	↓	↓	↓
	.0322	.0721	1.724	25.0	↓	↓	↓	↓	↓	↓
	.0375	.0826	2.275	33.0	↓	↓	↓	↓	↓	↓
0.635-cm (0.25-in.) extension	0.0218	0.0480	1.331×10^5	19.3	0.925	0.1089	0.24	2.289×10^6	332	0.828
	.0304	.0670	2.317	33.6	↓	↓	↓	↓	↓	↓
	.0458	.1010	4.482	65.0	↓	↓	↓	↓	↓	↓
Fuel injection angle										
Standard 0° impingement angle	0.0150	0.0332	0.710×10^5	10.3	0.9829	0.1089	0.24	2.172×10^6	315	0.8505
	.0246	.0543	1.434	20.8	↓	↓	↓	↓	↓	↓
	.0349	.0770	2.530	36.7	↓	↓	↓	↓	↓	↓
	.0183	.0404	.896	13.0	↓	↓	↓	↓	↓	↓
	.0297	.0654	1.896	27.5	↓	↓	↓	↓	↓	↓
	.0298	.0657	1.862	27.0	↓	.1043	.23	2.137	310	.8216
	.0377	.0831	2.717	39.4	↓	↓	↓	↓	↓	↓
	.0499	.1100	4.240	61.5	↓	↓	↓	↓	↓	↓
	15° impingement angle	0.0199	0.0439	1.069×10^5	15.5	0.9509	0.0998	0.22	2.075×10^6	301
.0258		.0569	1.641	23.8	↓	↓	↓	↓	↓	↓
.0346		.0763	2.620	38.0	↓	↓	↓	↓	↓	↓
.0387		.0854	3.158	45.8	↓	↓	↓	↓	↓	↓
.0297		.0654	2.124	30.8	↓	↓	↓	↓	↓	↓
30° impingement angle	0.0196	0.0433	1.289×10^5	18.7	0.8680	0.1043	0.23	2.103×10^6	305	0.8283
	.0275	.0606	2.296	33.3	↓	↓	↓	↓	↓	↓
	.0435	.0960	4.930	71.5	↓	↓	↓	↓	↓	↓
	.0307	.0678	2.723	39.5	↓	↓	↓	↓	↓	↓
45° impingement angle	0.0166	0.0366	1.875×10^5	27.2	0.6167	0.1043	0.23	2.103×10^6	305	0.8283
	.0210	.0464	2.999	43.5	↓	↓	↓	↓	↓	↓
	.0304	.0670	5.075	73.6	↓	↓	↓	↓	↓	↓
	.0268	.0592	4.275	62.0	↓	↓	↓	↓	↓	↓
Oxidizer tube base thickness										
Standard thickness	0.0208	0.0458	0.951×10^5	13.8	1.05	0.0998	0.22	-----	---	---
	.0327	.0713	1.999	29.0	↓	↓	↓	↓	↓	↓
	.0423	.0933	3.227	46.8	↓	↓	↓	↓	↓	↓
	.0269	.0593	1.510	21.9	↓	↓	↓	↓	↓	↓
Blunt base	0.0195	0.0430	0.827×10^5	12.0	1.05	-----	---	-----	---	---
	.0301	.0663	1.765	25.6	↓	↓	↓	↓	↓	↓
	.0428	.0944	3.047	44.2	↓	↓	↓	↓	↓	↓
	.0236	.0521	1.165	16.9	↓	↓	↓	↓	↓	↓
	.0366	.0807	2.406	34.9	↓	↓	↓	↓	↓	↓
Thin base	0.0146	0.0321	0.552×10^5	8.0	1.05	-----	---	-----	---	---
	.0288	.0636	1.655	24.0	↓	↓	↓	↓	↓	↓
	.0388	.0856	2.710	39.3	↓	↓	↓	↓	↓	↓
	.0361	.0795	2.434	35.3	↓	↓	↓	↓	↓	↓
	.0317	.0700	1.944	28.2	↓	↓	↓	↓	↓	↓

TABLE IV. - RESPONSE FACTOR INPUTS

[Time delay constant for burning, τ , 0.00008 sec; $\Delta\tau$, 0.00001 sec; oxidant-fuel ratio, 5.0; chamber pressure, 2.06×10^6 N/m² (300 psi); propellant flow rate, 29.48 kg/sec (65.0 lb/sec); $\gamma = C_p/C_v = 1.2$; hydrogen density, 3.2 to 64.1 kg/m³ (0.2 to 4.0 lb/ft³).]

Configuration	Hydrogen annulus entrance area, A ₁		Effective H ₂ injection area, A _{eff}		Hydrogen dome volume, V _H		Ratio of hydrogen annulus length to cross-sectional area, L/A		Screech frequency, f, Hz	Actual H ₂ injection area, A _{meas}		Hydrogen flow coefficient, (C _d) _N
	cm ²	in. ²	cm ²	in. ²	cm ³	in. ³	L/A			cm ²	in. ²	
							1/cm	1/in.				
Standard 0° impingement angle	78.90	12.23	18.000	2.790	1376.5	84.0	0.0429	0.1090	3284	18.594	2.882	0.968
15° impingement angle	↓	↓	17.032	2.640	↓	↓	.0378	.0960	↓	↓	↓	.916
30° impingement angle	↓	↓	15.206	2.357	↓	↓	.0401	.1018	↓	↓	↓	.818
45° impingement angle	↓	↓	14.729	2.283	↓	↓	.0443	.1124	↓	↓	↓	.792
Thin base	↓	↓	16.677	2.585	↓	↓	.0429	.1090	3333	↓	↓	.897
Blunt base	↓	↓	17.890	2.773	↓	↓	.0429	.1090	3310	↓	↓	.962
0.064-cm (0.025-in.) extension	↓	↓	18.355	2.845	↓	↓	.0737	.1873	3300	↓	↓	.987
0.254-cm (0.10-in.) recess	↓	↓	15.006	2.326	↓	↓	.0601	.1526	3300	↓	↓	.806
0.508-cm (0.20-in.) recess	↓	↓	14.652	2.271	↓	↓	.0464	.1179	3323	↓	↓	.788
0.84-cm (0.33-in.) recess ^a	↓	↓	5.374	.833	↓	↓	.0287	.0728	3333	↓	↓	.289
Flush	58.84	9.12	26.393	4.091	753.8	46.0	.0273	.0693	3400	29.787	4.617	.886
0.238-cm (0.094-in.) recess	↓	↓	16.110	2.497	↓	↓	.0188	.0477	3383	31.226	4.840	.516
0.762-cm (0.30-in.) recess	↓	↓	13.703	2.124	↓	↓	.0273	.0693	3277	29.787	4.617	.460
1.27-cm (0.50-in.) recess ^a	↓	↓	6.432	.997	↓	↓	.0273	.0693	3150	29.787	4.617	.216

^aStable.



CD-7999

Figure 1. - Engine mounted on thrust stand.

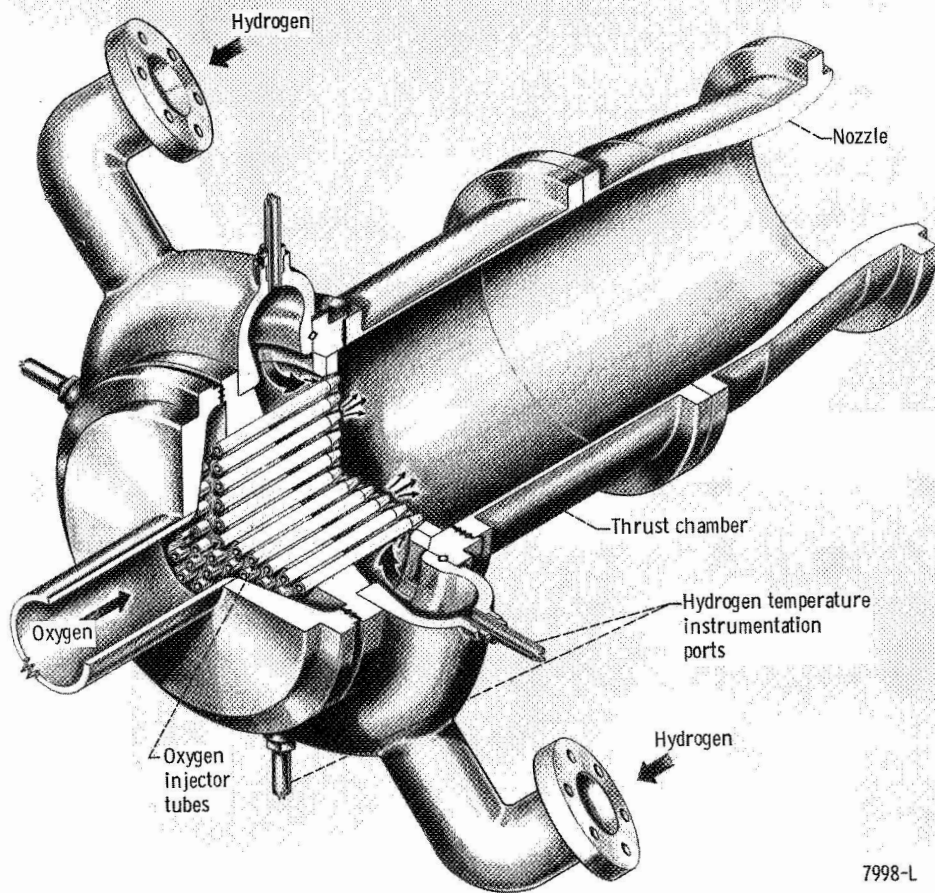
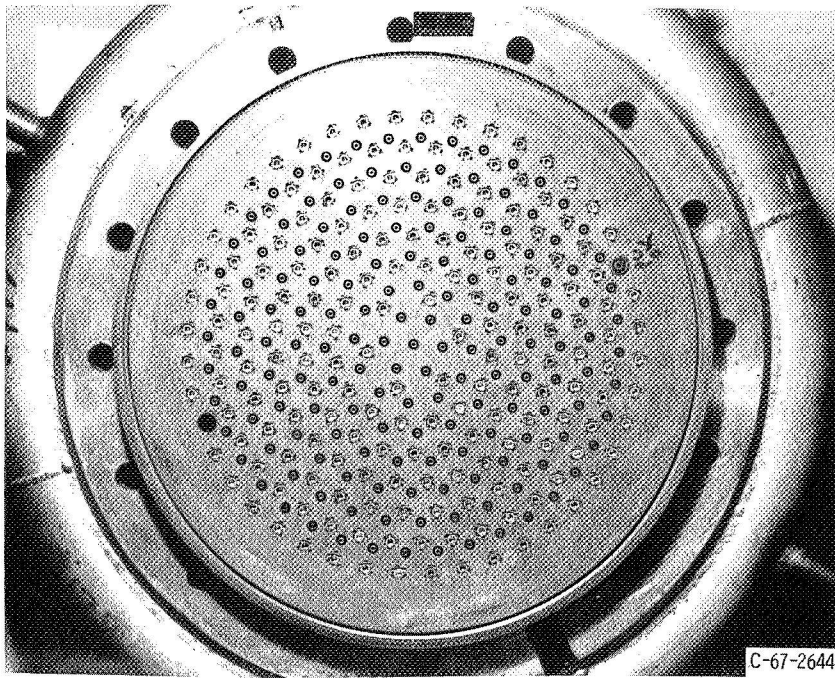
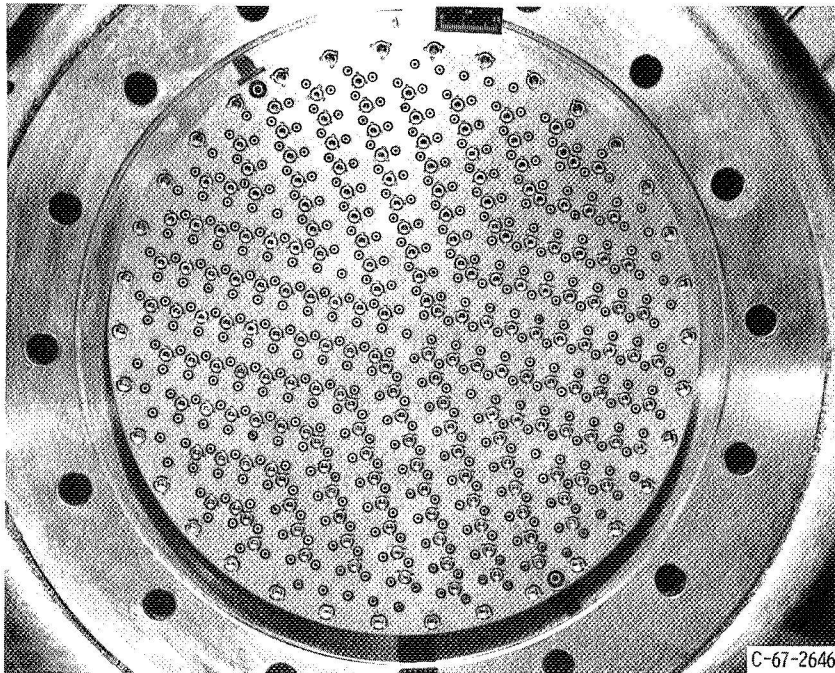


Figure 2 - Rocket engine.



(a) 157 Element.



(b) 421 Element.

Figure 3. - Injector faceplate view.

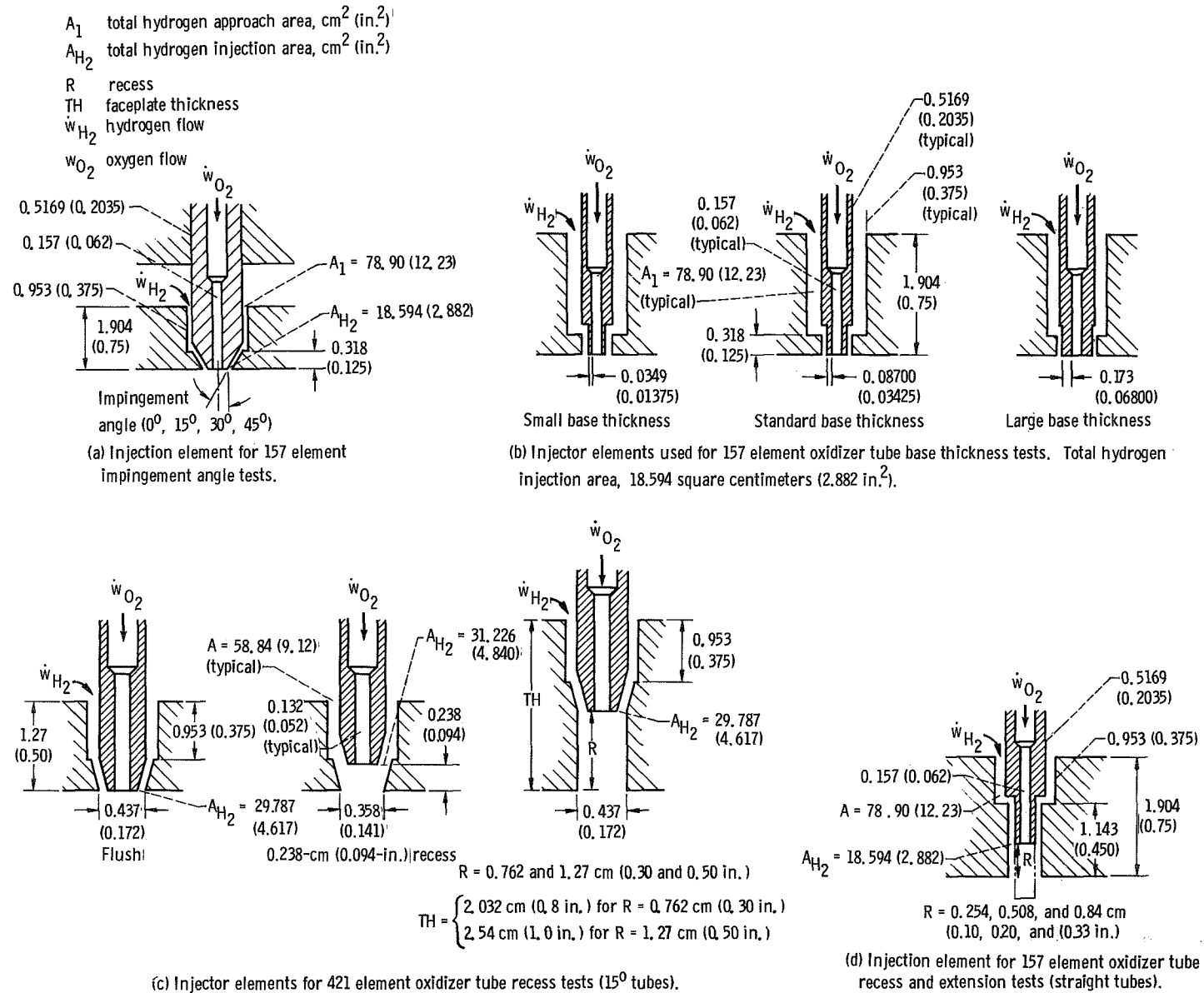
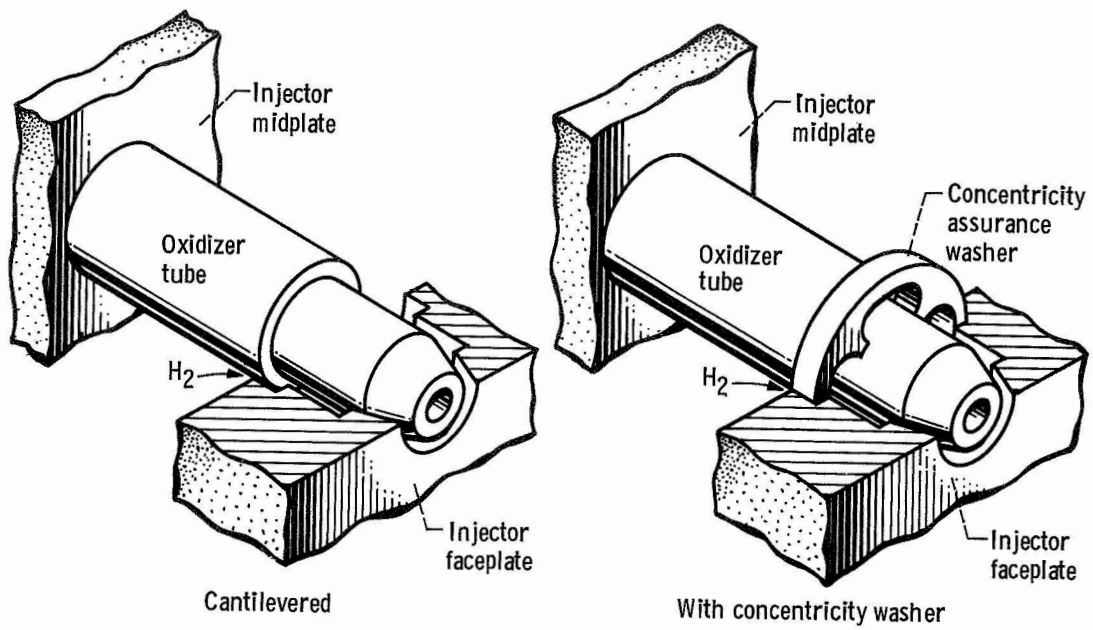
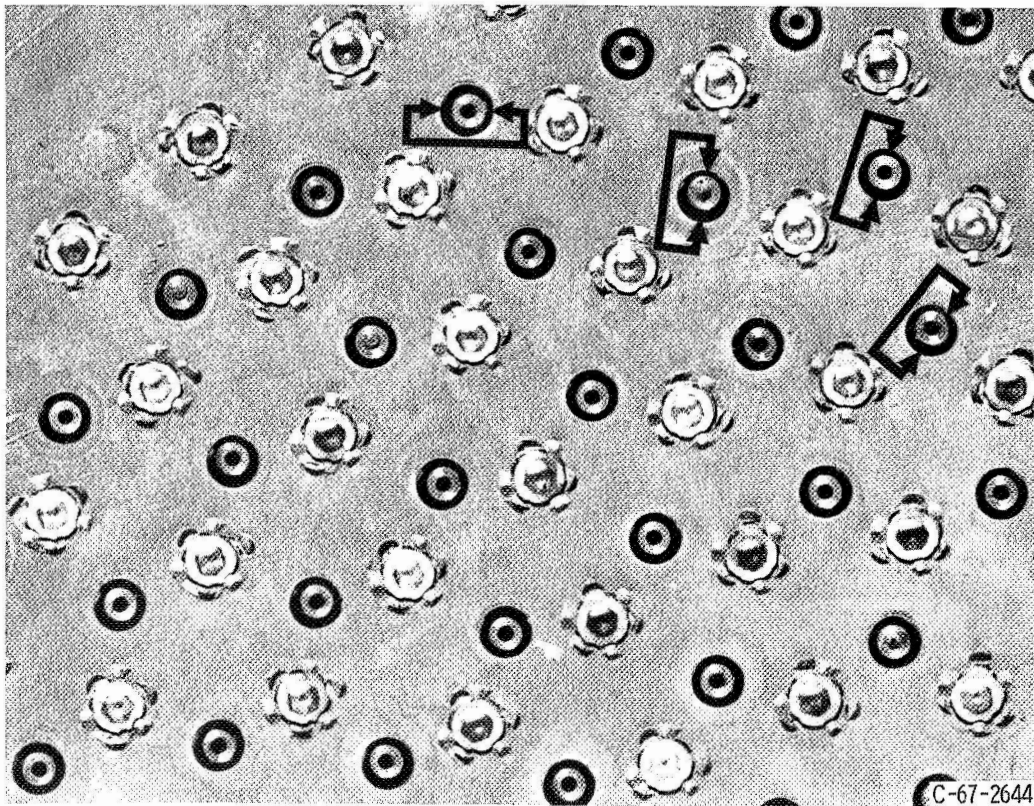


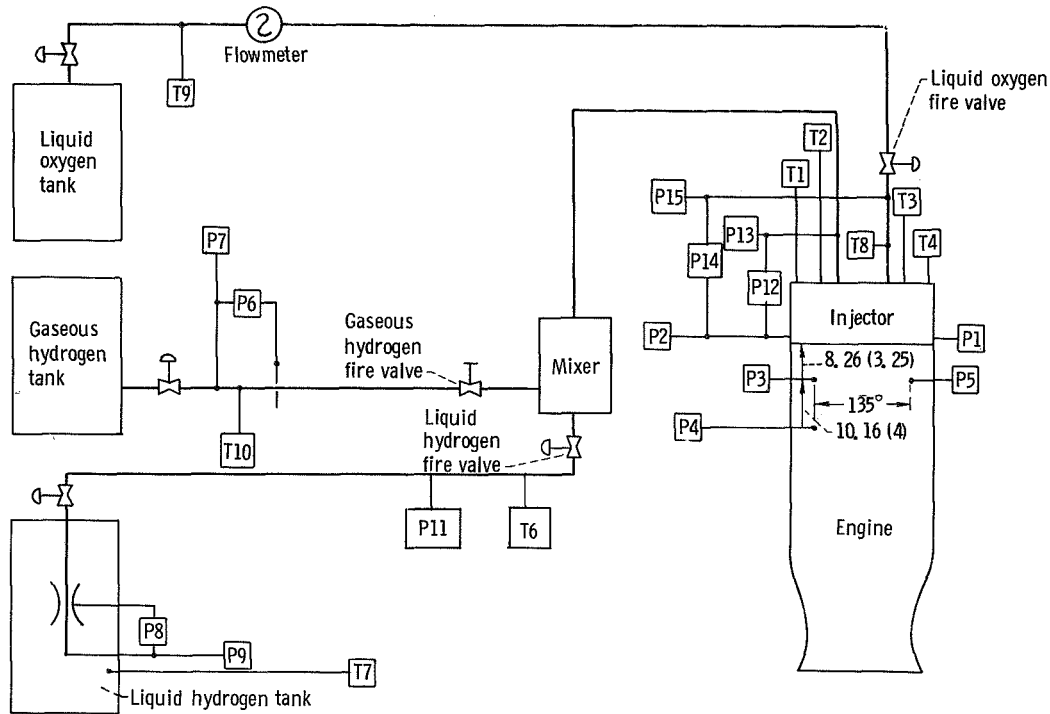
Figure 4 - Details of injector elements. (Dimensions in cm (in.) unless indicated otherwise).



(e) Element details used to examine effects of concentricity.



(f) Closeup view of 157 element injector without concentricity washers.
Figure 4. - Concluded.



- | | | | |
|-----|---|-----|---|
| P1 | Static chamber pressure (injector face), four-arm strain-gage transducer 1 | P14 | Oxygen injection differential pressure, four-arm strain-gage transducer |
| P2 | Static chamber pressure (injector face), four-arm strain-gage transducer 2 | P15 | Oxygen injection pressure, four-arm strain-gage transducer |
| P3 | Dynamic chamber pressure, water-cooled quartz pressure transducer 3 | T1 | Hydrogen injector temperature, carbon resistor sensor probe 1 |
| P4 | Dynamic chamber pressure, water-cooled quartz pressure transducer 4 | T2 | Hydrogen injector temperature, carbon resistor sensor probe 2 |
| P5 | Dynamic chamber pressure, water-cooled quartz pressure transducer 5 | T3 | Hydrogen injector temperature, carbon resistor sensor probe 3 |
| P6 | Gaseous hydrogen orifice differential pressure, four-arm strain-gage transducer | T4 | Hydrogen injector temperature, carbon resistor sensor probe 4 |
| P7 | Gaseous hydrogen orifice pressure, four-arm strain-gage transducer | T5 | Hydrogen mixer temperature, carbon resistor sensor probe |
| P8 | Liquid hydrogen venturi differential pressure, four-arm strain-gage transducer | T6 | Liquid hydrogen line temperature, carbon resistor sensor probe |
| P9 | Liquid hydrogen venturi pressure, four-arm strain-gage transducer | T7 | Liquid hydrogen venturi temperature, platinum resistance thermometer |
| P10 | Hydrogen mixer pressure, four-arm strain-gage transducer | T8 | Oxygen injection temperature, copper-constantan thermocouple |
| P11 | Liquid hydrogen line pressure, four-arm strain gage transducer | T9 | Oxygen flowmeter temperature, platinum resistance thermometer |
| P12 | Hydrogen injection differential pressure, four-arm strain-gage transducer | T10 | Gaseous hydrogen orifice temperature, iron-constantan thermocouple |
| P13 | Hydrogen injection pressure, four-arm strain-gage transducer | | |

Figure 5. - Instrumentation diagram. (Dimensions in cm (in.) unless indicated otherwise.)

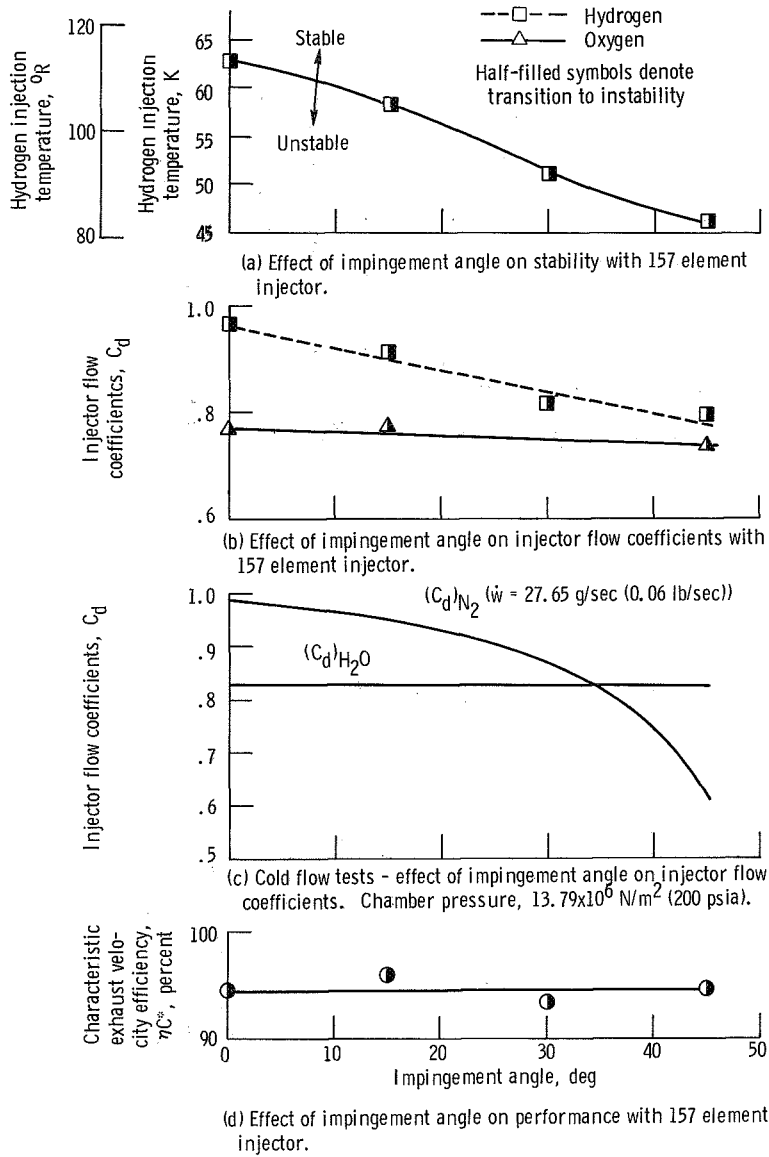


Figure 6. - Effect of impingement angle on stability limits, injector flow coefficients, and performance with 157 element injector oxidant-fuel ratio, 5.0.

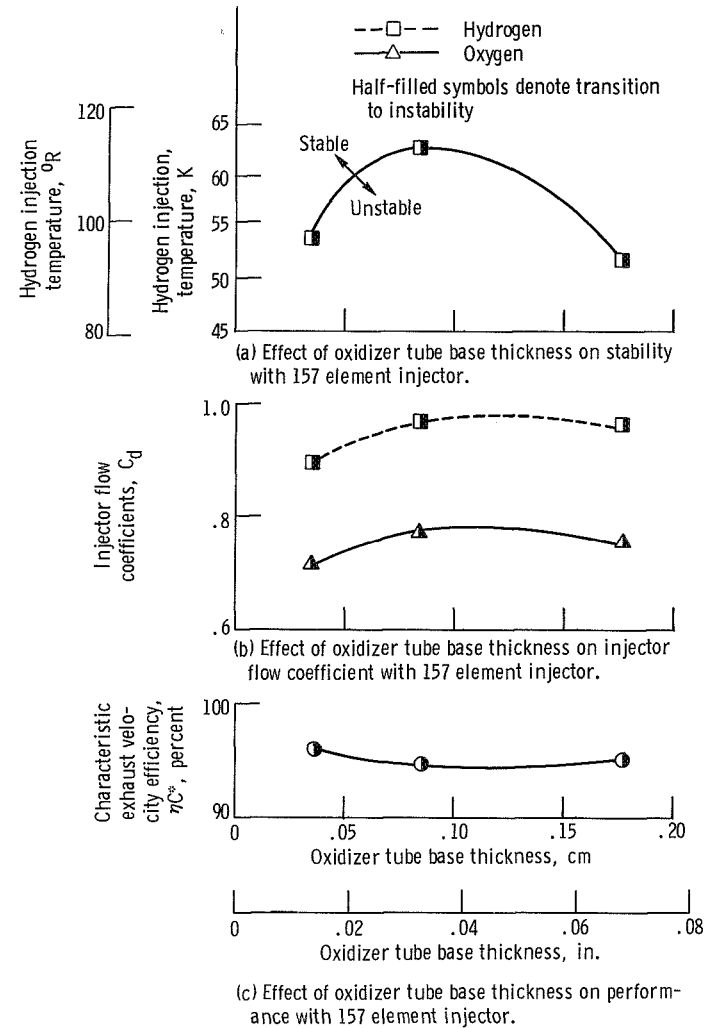


Figure 7. - Effect of oxidizer tube base thickness on stability limits, injector flow coefficients, and performance with 157 element injector. Oxidant-fuel ratio, 5.0.

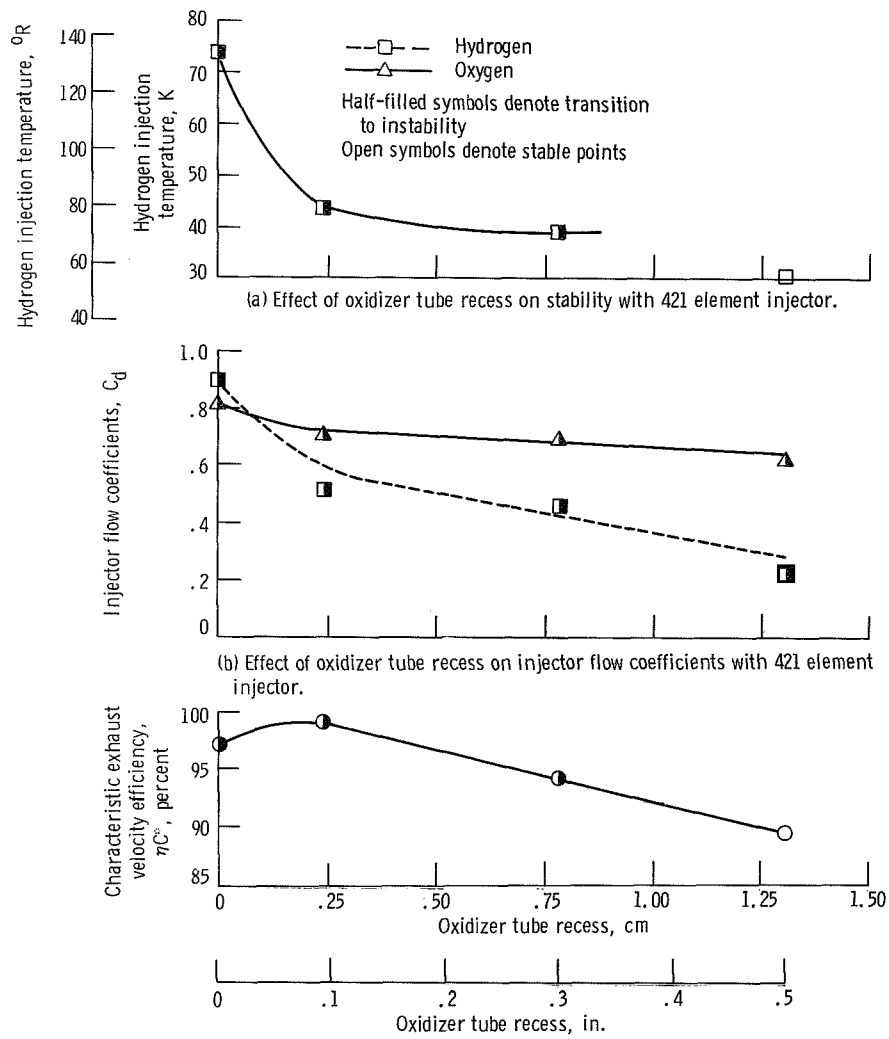
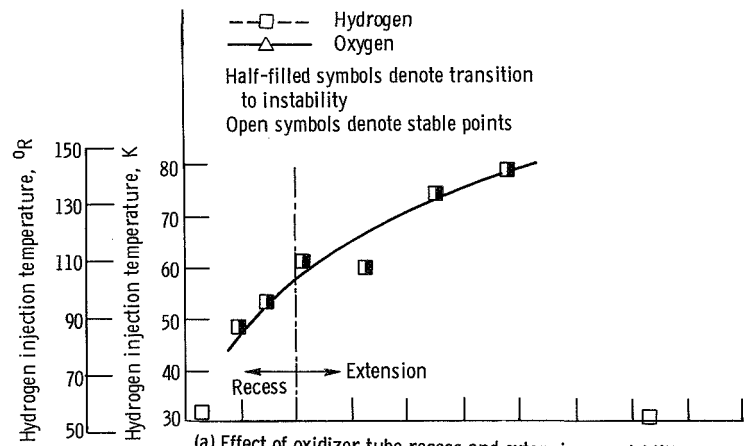
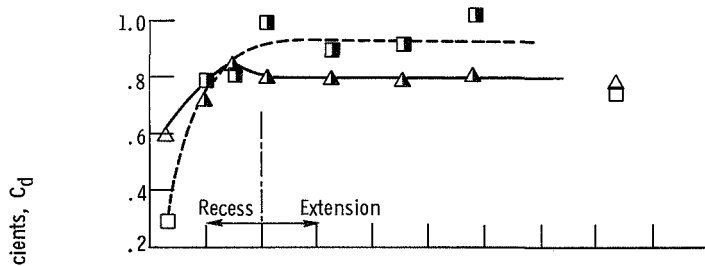


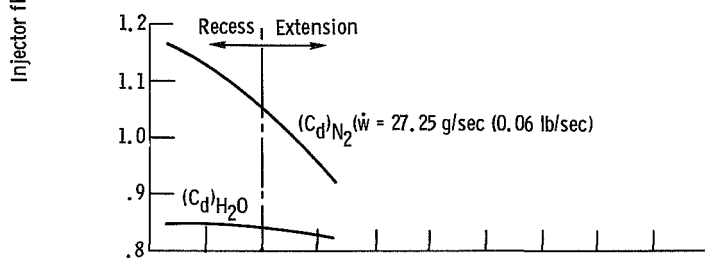
Figure 8. - Effects of oxidizer tube recess on stability limits, injector flow coefficients, and performance with 421 element injector. Oxidant-fuel ratio, 5.0.



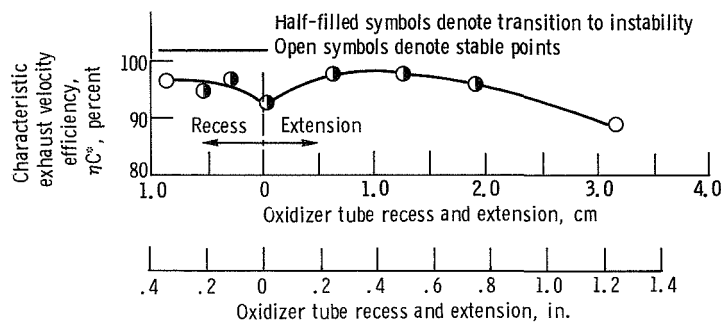
(a) Effect of oxidizer tube recess and extension on stability with 157 element injector.



(b) Effect of oxidizer tube recess and extension on injector flow coefficients with 157 element injector.



(c) Cold flow tests - effect of oxidizer tube recess and extension on injector flow coefficients. Chamber pressure, $13.79 \times 10^6 \text{ N/m}^2$ (200 psia).



(d) Effect of oxidizer tube recess and extension on performance with 157 element injector.

Figure 9. - Effect of oxidizer tube recess and extension on stability limits, injector flow coefficients with 157 element injector. Oxidant-fuel ratio, 5.0.

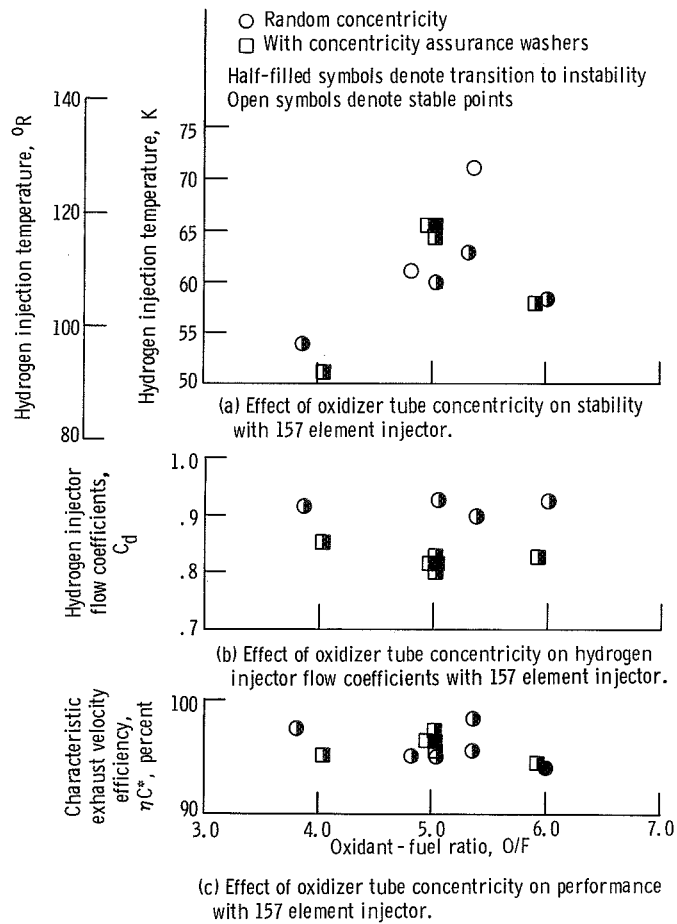


Figure 10. - Effect of oxidizer tube concentricity on stability limits, injector flow coefficients, and performance with 157 element injector. Oxidant-fuel ratio, 5.0.

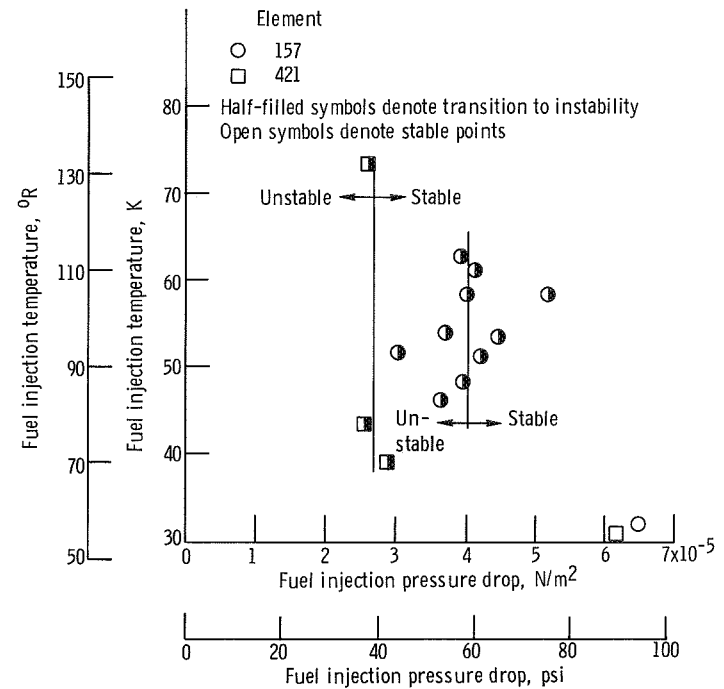


Figure 11. - Fuel injection differential pressure as a correlating parameter.

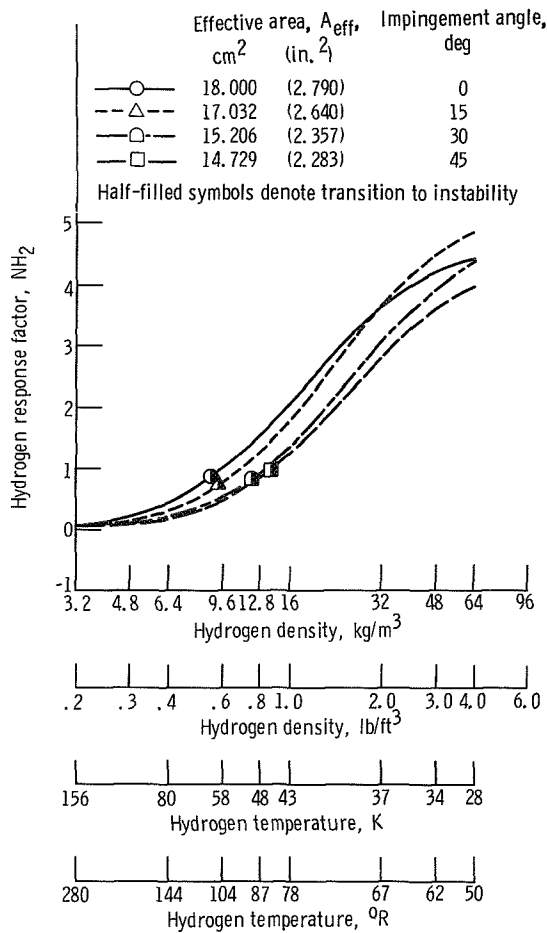


Figure 12. - 157 Element impingement angle response factor. Time, 0.00008 second; oxidant-fuel ratio, 5.0; chamber pressure, 2.06×10^6 N/m² (300 psi); propellant flow rate, 29.48 kilograms per second (65.0 lb/sec).

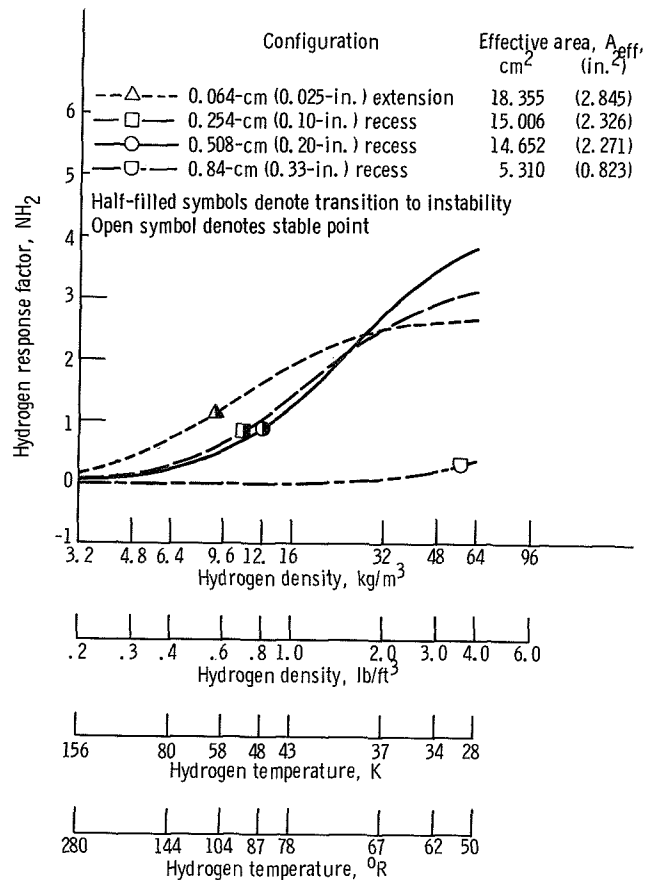


Figure 13. - 157 Element recess response factor. Time, 0.00008 second; oxidant-fuel ratio, 5.0; chamber pressure, 2.06×10^6 N/m² (300 psi); propellant flow rate, 29.48 kilograms per second (65.0 lb/sec).

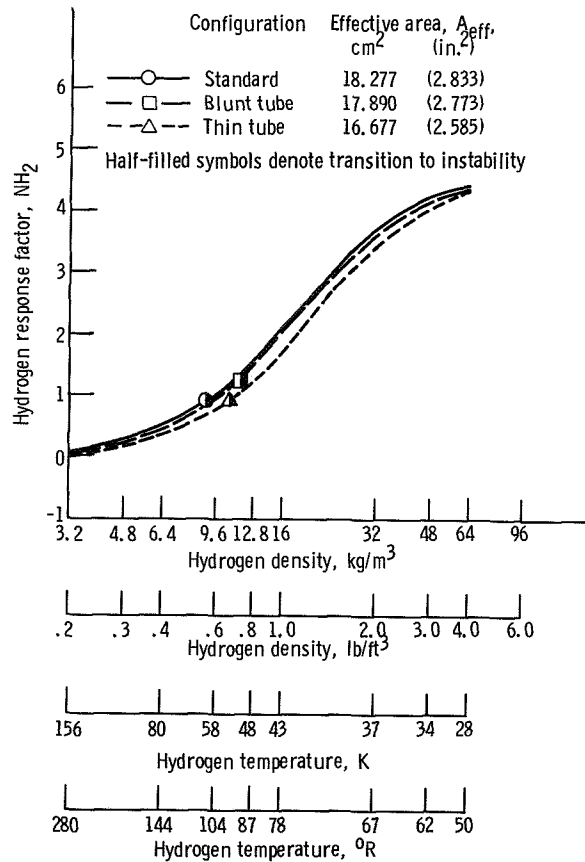


Figure 14. - 157 Element base thickness response factor. Time, 0.00008 second; oxidant-fuel ratio, 5.0; chamber pressure, 2.06×10^6 N/m² (300 psi); propellant flow rate, 29.48 kilograms per second (65.0 lb/sec).

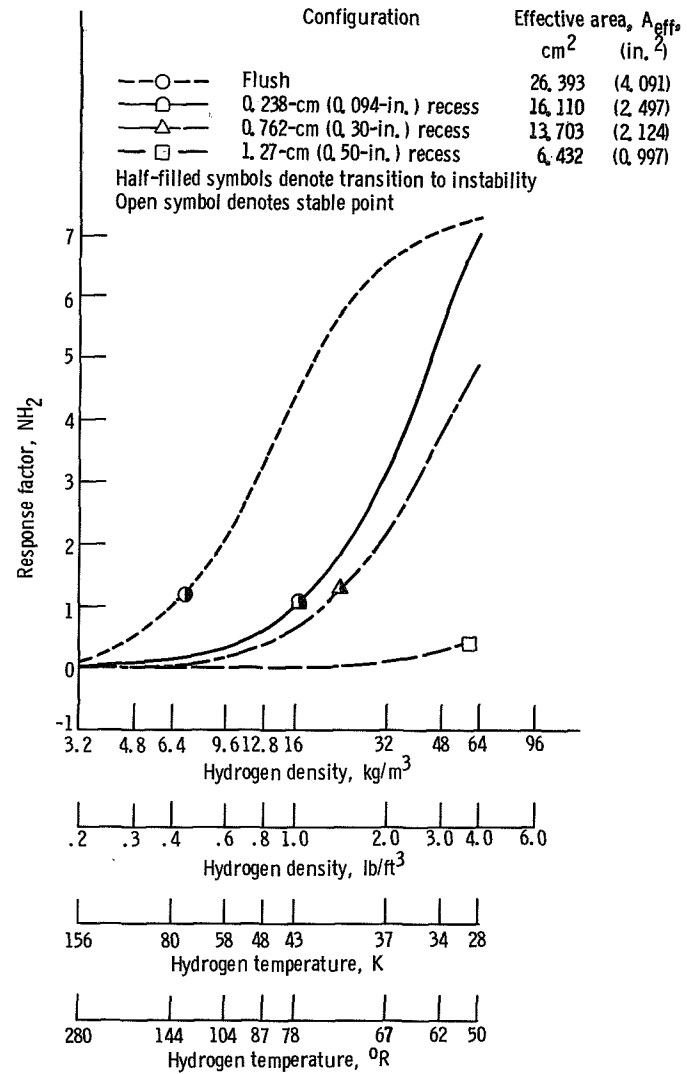


Figure 15. - 421 Element recess response factor. Time, 0.00008 second; oxidant-fuel ratio, 5.0; chamber pressure, 2.06×10^6 N/m² (300 psi); propellant flow rate, 29.48 kilograms per second (65.0 lb/sec).

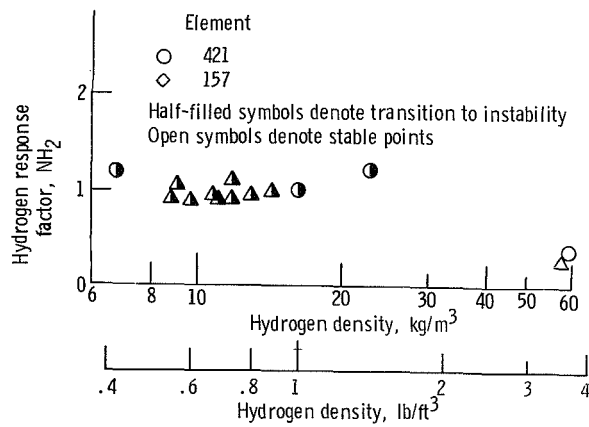


Figure 16. - Correlation of element detail data with hydrogen response factor.

NATIONAL AERONAUTICS AND SPACE ADMINISTRATION
WASHINGTON, D.C. 20546

OFFICIAL BUSINESS
PENALTY FOR PRIVATE USE \$300

**SPECIAL FOURTH-CLASS RATE
BOOK**

POSTAGE AND FEES PAID
NATIONAL AERONAUTICS AND
SPACE ADMINISTRATION
451



POSTMASTER: If Undeliverable (Section 158
Postal Manual) Do Not Return

"The aeronautical and space activities of the United States shall be conducted so as to contribute . . . to the expansion of human knowledge of phenomena in the atmosphere and space. The Administration shall provide for the widest practicable and appropriate dissemination of information concerning its activities and the results thereof."

—NATIONAL AERONAUTICS AND SPACE ACT OF 1958

NASA SCIENTIFIC AND TECHNICAL PUBLICATIONS

TECHNICAL REPORTS: Scientific and technical information considered important, complete, and a lasting contribution to existing knowledge.

TECHNICAL NOTES: Information less broad in scope but nevertheless of importance as a contribution to existing knowledge.

TECHNICAL MEMORANDUMS: Information receiving limited distribution because of preliminary data, security classification, or other reasons. Also includes conference proceedings with either limited or unlimited distribution.

CONTRACTOR REPORTS: Scientific and technical information generated under a NASA contract or grant and considered an important contribution to existing knowledge.

TECHNICAL TRANSLATIONS: Information published in a foreign language considered to merit NASA distribution in English.

SPECIAL PUBLICATIONS: Information derived from or of value to NASA activities. Publications include final reports of major projects, monographs, data compilations, handbooks, sourcebooks, and special bibliographies.

TECHNOLOGY UTILIZATION PUBLICATIONS: Information on technology used by NASA that may be of particular interest in commercial and other non-aerospace applications. Publications include Tech Briefs, Technology Utilization Reports and Technology Surveys.

Details on the availability of these publications may be obtained from:

SCIENTIFIC AND TECHNICAL INFORMATION OFFICE

NATIONAL AERONAUTICS AND SPACE ADMINISTRATION

Washington, D.C. 20546